1-1-2011

Electronic excitations in branched conjugated oligomers: A quasiparticle view and tight-binding models

Hao Li

Wayne State University,

ELECTRONIC EXCITATIONS IN BRANCHED CONJUGATED OLIGOMERS: A QUASIPARTICLE VIEW AND TIGHT-BINDING MODELS

by

HAO LI

DISSERTATION

Submitted to the Graduate School

of Wayne State University,

Detroit, Michigan

in partial fulfillment of the requirements

for the degree of

DOCTOR OF PHILOSOPHY

2011

MAJOR: CHEMISTRY (Physical)

Approved by:

_____

Advisor Date

_____

_____

_____

_____

DEDICATION

This dissertation is dedicated to my daughter Katherine

ACKNOWLEDGEMENTS

This dissertation could hardly have been possible without the support and assistance of many people. It is my pleasure to take this opportunity to thank all those people who have contributed to this dissertation and encouraged me throughout the research.

First, I would like to express my profound gratitude to my research supervisor Professor Vladimir Chernyak, for all of his invaluable guidance, assistance and inspiration throughout my graduate study at Wayne State University. I am amazingly fortunate to have an advisor who provides a well-rounded experience consistent with my long-term academic career as well as academic guidance. His talent and enthusiasm in science made this dissertation happened.

I am deeply grateful to Dr. Sergei Tretiak for the useful discussions and contributions throughout this work. It is my great pleasure and cherished experience to be a summer graduate student with him during the past two years. I am also thankful to him for teaching me all the techniques of computation chemistry as well as insights on scientific research in general.

My thanks also go to the current and superior members of Chernyak research group for their assistance and friendship. Especially, I would like to thank Dr. Sergey Malinin for his assistance in both the theoretical work and all technical details of this research. His help in improving my writing and presentations is highly appreciated. The friendship of Dr. Chao Wu is much appreciated and has led to many interesting and spirited discussions relating to this research.

Most calculations were performed using the resources of the Grid of Wayne State University and Center for Integrated Nanotechnologies of Los Alamos National Laboratory, which are gratefully acknowledged.

Finally, I would like to thank my wife Xiaobin Zhu for her love, understanding, support and sacrifices during the past ten years. My parents Yunqi Li and Fenglan Ji receive my deepest gratitude for their dedication and many years of support. The unwavering love and faith from my wife and my parents is what has shaped me to be the person I am today. Thank you for everything.

TABLE OF CONTENTS

LIST OF TABLES

LIST OF FIGURES

Chapter 1

Introduction

Understanding and simulation of the excited-state electronic structure of organic molecules are important tasks in physical chemistry and material science because light absorption, emission, and photoinduced energy transfer are all determined by the structure of the electronic excitations. Besides improving the microscopic insights into photophysics and photochemisty, these studies play important roles in developing new electro-optical materials.

Carbon-rich molecular structures may exhibit remarkable electronic and optical properties [2–12] due to the high degree of $\pi-$conjugation. Such conjugated molecules have been intensively studied for their interesting photophysical and carrier transport properties, as well as technological advantages over traditional semiconductors [13–15]. Therefore, branched conjugated molecules have an increasing number of applications as organic photovoltaic materials, e.g. organic light-emitting diodes [16], single-molecule switches [17], organic solar cells [18], transistors [19–21], and imaging devices [21–23]. In the past three decades, a number of branched conjugated polymers and networks with various building blocks have been synthesized, including structures based on phenylacetylene, thiophene, phenylenevinylene, phenylbutadiyne, etc., that can also be decorated with side groups and attached to nanoparticles [24–34]. The geometry of branched conjugated molecules is a key factor for their optical applications. The efficiency of light absorption can be improved by a high concentration of peripheral chromophores in the branched structures. Selective light absorption and directed energy transport can be achieved using different molecular geometries,

purposing proper transition dipole moments and energetic gradients [10, 35–37]. Therefore, understanding the excited-state electronic structure in conjugated molecules and underlying structure-property relations is a nontrivial task and important for the design of novel organic photovoltaic materials.

The complicated electronic structure of conjugated molecules has been attributed to the quasi-one-dimensional system of delocalized $\pi-$electrons subject to strong Coulomb electron-electron correlations and electron-phonon couplings [13, 14, 36]. Therefore, large conjugated molecules are very difficult to study theoretically with both satisfactory efficiency and accuracy, especially when the properties involve excited electronic states. The latter typically correspond to tightly bound electron-hole pairs (excitons) due to the low-dimensionality and a low dielectric constant in these materials. Using general quantum chemistry methods, the numerical cost [which scales as O(N^2) - O(N^5), N being the number of orbitals] makes computations for large molecules with hundreds and thousands of atoms prohibitively expensive [38]. Fortunately, the excited-state computation can be simplified by a quasiparticle (exciton) description, the exciton scattering (ES) approach [36, 39], prompted by the context of electron energy loss spectroscopy [40, 41].

The ES approach has been developed for numerically efficient calculations of optical spectra in large branched conjugated molecules [36, 42], where electronic excitations are represented by excitons. This approach is based on the following simple and physically intuitive picture: electronic molecular excitations are viewed as states of a quantum particle on the graph whose edges and vertices represent linear segments and vertices of the molecule. Therefore, finding transition energies and exciton wave functions is similar to a much simpler and computationally inexpensive problem of finding the eigenstates of a quantum particle on the graph (a "particle in a box" problem): one needs to solve a set of homogeneous wave equations (ES equations) describing quantum scattering at the vertices and propagation along linear segments. The ES approach was put on a firm theoretical basis [42] as an approximation that becomes asymptotically exact in the limit when the linear segments are

much longer than the exciton size. In the infinite linear chain the exciton quasimomentum k is conserved, and the dispersion relation $\omega(k)$ (dependence of the transition energy ω on k) characterizes the polymer backbone. Molecular vertices locally violate the discrete translational symmetry and cause exciton scattering described by ω-dependent scattering matrices $\Gamma^{(n)}(\omega)$ (a unitary symmetric $n \times n$ matrix characterizes a vertex of degree n); the exciton wave function is a standing wave at distances larger than the exciton size. All these ES parameters can be obtained from the reference quantum-chemical computations (from the transition energies, by solving an inverse scattering problem, or by extracting standing-wave envelopes from the transition density matrices) in molecules of moderate size and tabulated for further applications. In Refs. [39, 43] a strategy for retrieving the scattering matrices have been developed: first, the exciton dispersion together with the scattering amplitude at the molecular termini, and next, the 2×2 scattering matrices for double joints from quantum-chemical results. This strategy was implemented for both the time-dependent density functional [39] and time-dependent Hartree-Fock [43] methods using an example of phenylacetylene (PA, or poly phenylene ethynylene, PPE) systems [7, 8] including unmodified chain termini, as well as *ortho*- and *meta*-joints. The accuracy of the ES approach has been checked by comparing the excitation energies obtained via solving the ES equations, using the retrieved ES parameters, with the quantum-chemical calculations in a variety of test molecules. For all PA-based molecules studied thus far, the ES approach produced impressively accurate results [39, 44].

For large branched conjugated molecules, finding numerical solutions of the ES equations is much more efficient than application of the reference quantum-chemical method. Indeed, such a large molecule typically contains large numbers but only several types of building blocks; using the same ES parameters for the same building blocks effectively accounts for this symmetry. The ES approach can efficiently calculate transition frequencies for all possible branched conjugated molecules composed of characterized building blocks as well as the reference quantum chemistry would do if it were not for limitations imposed by

computational expense. Ultimately, the quasiparticle description of the ES approach can serve as a foundation for treating effects of disorder and exciton-phonon interactions, which is necessary for efficient modeling of energy transfer in conjugated systems.

This dissertation further extends the ES approach to allow for numerically efficient calculations of optical spectra and vibrational dynamics in large molecular systems. In Chapter 2, we extend the ES approach to the calculation of the transition dipole moments. The formalism for this extension is presented based on the generalized ES approach. The dipole properties of building blocks are fully characterized by several energy-dependent ES parameters. These dipole ingredients have been retrieved from the quantum-chemical calculations of the excited states in simple molecular fragments. Using these extracted parameters, one can then effortlessly calculate the oscillator strengths and optical spectra of various large molecular structures. We illustrate the application of this extended ES approach using an example of phenylacetylene-based molecules. Absorption spectra predicted by the ES approach have been compared with the results of the reference quantum-chemical calculations to check the accuracy.

In Chapter 3, the ES methodology is extended to analyze the excited-state electronic structure of donor and acceptor substituted conjugated oligomers, which provide an important approach to modify the optical properties of the backbone structures. The extracted ES parameters (including the scattering phases, the transition charge and dipole ingredients) of the modified termini are used to quantify the influence of the substitution on the molecular electronic and optical spectra. In particular, intuitive relationships between the substituent's electron withdrawing or donating ability and the exciton scattering parameters are discussed. Good agreement of the absorption spectra between the ES approach and the reference quantum-chemical computations demonstrates that the ES approach is qualified for such conjugated push-pull molecular systems.

In Chapter 4 the capability of the ES approach is extended to include symmetric triple and quadruple joints that connect linear segments based on the phenylacetylene backbone. This

allows us to extend the ES methodology to a much broader variety of branched conjugated molecules and molecular networks that consist of the characterized building blocks. The symmetric double joints have been restudied in terms of the symmetry. Then we present initial studies of the analytical properties of the scattering matrices $\Gamma(\omega)$ and, in particular, relate some simple topological invariants, associated with $\Gamma(\omega)$, to the number of electronic excitations in the conjugated molecules that contain the corresponding joints. The obtained features of the scattering phases are analyzed in terms of the observed excited-state electronic structure. The topological approach is very useful in counting the exciton states inside the exciton band.

In Chapter 5, we introduced an efficient description of electronic excitations in terms of effective tight-binding (lattice) models whose parameters are determined from the behavior of the ES parameters. Application is illustrated by constructing lattice models for two types of excitons in linear phenylacetylene oligomers on the basis of the time-dependent Hartree-Fock computations. In particular, using the analytical continuation of the expression for the effective terminal reflection amplitude, we are able to accurately predict the energies of the bound states localized at the molecular vertices including the acceptor- and donor-substituted chain termini, symmetric quadruple joint, and perylene substituted terminus. In addition, the lattice models can be useful to determine the exciton-phonon coupling and the effect of disorder on electronic excitations in large branched conjugated molecules.

Finally the main conclusions of this dissertation are summarized in Chapter 6.

Chapter 2

Transition dipoles and optical spectra of conjugated molecules

The energies of electronic excitations constitute an important piece of information for describing optical properties of materials, because they indicate the positions of the absorption peaks. However, the optical properties also depend on the transition dipole moments of excited states. These quantities determine whether respective electronic transitions carry oscillator strengths that define the intensities of the corresponding peaks in the optical spectra[45]. In this chapter, we generalize the formalism of the exciton scattering (ES) approach for electronic excitations in branched conjugated molecules and extend it to the calculation of transition dipole moments. Together with the original ES approach developed previously [36, 39, 42–44], this extension allows one to calculate efficiently optical spectra in large conjugated molecules using previously tabulated ES parameters obtained from quantum-chemical calculations of basic molecular building blocks.

In the context of the ES approach, the wave function for a stationary state of the "particle in a box" problem, which has a standing-wave form, should be interpreted as a distribution of the excitation amplitudes on the linear segments. The idea behind the calculation of transition dipoles within the ES approach is that the contribution of a building block to the total dipole is proportional to the local excitation amplitude. Specifically, transition charges and dipoles of building blocks can be determined using a small number of energy-dependent parameters. These dipole and charge parameters can also be extracted from the

reference quantum-chemical computations in molecules of moderate sizes and tabulated in addition to the scattering parameters for the excitation energies. Consequently, the transition dipole moment magnitudes can be computed efficiently for any molecule that consists of characterized building blocks, similarly to computation of excitation energies within the ES approach. Excitation energies and transition dipole moments allow us to calculate optical spectra. On several examples of phenylacetylene π-conjugated molecular structures [8, 46–50], we found that the absorption spectra predicted by our extended ES approach accurately reproduce the results of the respective direct quantum-chemical calculations.

2.1 Transition dipoles within the ES approach

2.1.1 Generalized ES approach

In this section we review and generalize the exciton scattering (ES) approach. In conjugated molecules, the electronic excitations are tightly bound spatially localized excitons. Within the ES approach, an excitation in a conjugated molecule is viewed as a quantum particle (exciton) on the corresponding graph that represents the molecule (the molecular vertices and linear segments are represented by the vertices and edges of the graph). We assume that the properties of the molecular building blocks (repeat units and molecular vertices) depend only on the energy. In an infinite linear segment, the common motion of an electron and a hole that form the exciton, is described by a plane wave parameterized by the exciton quasimomentum. The spatial distribution of delocalized electronic excitation in a complex branched conjugated molecule can be characterized by the exciton wave function given by a set of standing waves on molecular linear segments α:

$$\psi_\alpha(x_\alpha) = a_\alpha \exp(ikx_\alpha) + b_\alpha \exp(-ikx_\alpha)\,, \tag{2.1}$$

where the wavenumber k is related to the excitation energy ω through the dispersion relation $\omega(k)$, and the wave function is defined at integer points x_α. Note that the excited state has a standing-wave structure only sufficiently far from the molecular vertices (in comparison

with the exciton size), which implies that the ES approach can be justified only if molecular linear segments are long compared to the typical distance between the electron and the hole in the exciton (exciton size).

In the following, to simplify the description, we assume that at a given energy there is only one exciton type. We choose to formulate the ES approach using the standing wave associated with the transition dipole distribution in real space, which has substantial intuitive advantage: as for a quantum particle, for the first excitation in the linear molecule this exciton wave function is symmetric and has no nodes, whereas for the second excitation it is antisymmetric (with one node), etc. This choice implies that the exciton wave function should be defined as a vector that can be represented by a unit vector $\boldsymbol{n}_\alpha$ in the direction of the repeat unit's axis and a projection $\psi_\alpha(x_\alpha)$ on that axis:

$$\boldsymbol{\psi}_\alpha(x_\alpha) = \psi_\alpha(x_\alpha)\boldsymbol{n}_\alpha\,. \tag{2.2}$$

The first version of the ES approach[42] was formulated in terms of the projections of the wave function ψ. However, this approach, when applied to complex structures with loops, requires inverting signs of some elements of scattering matrices for certain positions of vertices in the graph. The reason for this complication was possible conflicts in structures with loops between orientations that were necessarily included in definitions of scattering matrices based on projections. The representation (2.2) is especially useful when the repeat units can be viewed as straight but $\boldsymbol{n}_\alpha$ can slowly vary from repeat unit to repeat unit, whereas the local projection $\psi_\alpha(x_\alpha)$ of the wave function is not affected by this weak deformation.

Within the ES approach, the excitation amplitude can be found by solving simple wave equations describing propagation along linear segments and scattering at vertices. These equations, referred to as ES equations, can be formulated in terms of the incoming and outgoing waves $\psi_{\alpha b}^{(\pm)}$ defined as the values of two plane-wave components of the asymptotic standing wave continued to the vertex. In this notation incoming (+) and outgoing (-) waves are specified in the linear segment α at the vertex b. Propagation along the segment α of

length l_α between the vertices b and c is expressed by the equation

$$\boldsymbol{\psi}_{\alpha b}^{(-)} = \boldsymbol{n}_{\alpha b}(\boldsymbol{n}_{\alpha c}, \boldsymbol{\psi}_{\alpha c}^{(+)}) \exp\left(ikl_\alpha\right) , \tag{2.3}$$

where we introduced unit vectors corresponding to the directions of the segment's ends (we define these unit vectors as the unit vectors of the first and last repeat units), and $(\cdot, \cdot)$ stands for the scalar product.

Scattering matrices $\Gamma(\omega)$ quantify scattering at the molecular vertices:

$$\boldsymbol{\psi}_{\alpha b}^{(+)} = \boldsymbol{n}_{\alpha b} \sum_{\beta \ni b} \Gamma_{b,\alpha\beta}(\omega)(\boldsymbol{n}_{\beta b}, \boldsymbol{\psi}_{\beta b}^{(-)}) . \tag{2.4}$$

We note that specifying directions on all segments connected to the vertex is necessary to describe the scattering.

If the exciton dispersion $\omega(k)$ and the energy-dependent scattering matrices for all vertices are known, from Eqs. (2.3) and (2.4) one can find the excitation energies and the exciton wave function up to a normalization factor. We assume the following normalization condition of the exciton wave function

$$\sum_{\alpha \in \mathcal{M}_1} \sum_{x_\alpha = 1}^{l_\alpha} \psi_\alpha(x_\alpha)\psi_\alpha^*(x_\alpha) = 1. \tag{2.5}$$

The amplitudes of the exciton wave function ψ_α are directly related to the transition density matrices obtained in quantum-chemical calculation[42], which reflect changes in the single electron density matrix[51] due to optical excitation. The matrix elements of the transition density matrix between the ground state $|g\rangle$ and excited state $|\nu\rangle$ many-electron wave functions are defined as

$$(\xi_\nu)_{nm} = \langle \nu | c_n^\dagger c_m | g \rangle , \tag{2.6}$$

where $c_n^\dagger$ (c_m) are the Fermi creation (annihilation) operators for the n-th (m-th) basis set orbital. In the time dependent density functional theory (TDDFT) [52, 53] or time-dependent Hartree-Fock (TDHF)[54, 55] approximation the transition density matrices are obtained as eigenvectors diagonalizing an appropriate Liouville operator. These eigenvectors

in the orthonormal basis set are normalized with the condition

$$\mathrm{Tr}\,\left(\bar{\rho}[\xi_\nu^\dagger, \xi_\nu]\right) = 1\,, \tag{2.7}$$

where $\bar{\rho}$ represents the ground-state single-electron density matrix in the Hartree-Fock approximation[51, 56] or Kohn-Sham representation[57, 58]. This expression reduces to the usual scalar product in the Tamm-Dancoff approximation[59]. Consequently, the normalization condition of the exciton wave function (2.5) naturally follows from Eq. (2.7).

2.1.2 Calculation of the transition dipoles in the ES approach

To extend the ES approach to calculation of the transition dipole moments, we follow the way how they are calculated from the transition density matrix given in the basis of atomic orbitals, where the dipole matrices $\hat{\boldsymbol{\mu}}_{nm} = \langle n|\hat{\boldsymbol{\mu}}(\mathbf{r})|m\rangle$ are local (here $\hat{\boldsymbol{\mu}}(\mathbf{r})$ is the dipole operator)[56, 60]. After assuming for simplicity the orthogonality of the basis set orbitals, the transition dipole moment for optical excitation to state ν is defined as

$$\boldsymbol{\mu}_\nu = \mathrm{Tr}\,\left(\hat{\boldsymbol{\mu}}\xi_\nu\right)\,. \tag{2.8}$$

Eq. (2.8) basically involves a sum over all orbitals with the proper account of their overlapping. We separate the molecule into building blocks (repeat units and vertices) that occupy certain regions of space. Because the dipole matrices $\hat{\boldsymbol{\mu}}_{nm}$ are local (i.e., they have dominant block-diagonal structure with each block corresponding to the basis functions on the same atom), we can identify the transition charge and dipole of individual molecular units [42]. The building block's dipole is defined with respect to a point "attached" to the particular building block and chosen in the same way for all building blocks of this type.

For any wavenumber k, there are two linearly independent standing waves. One of them is the exciton wave function. The second standing wave $\tilde{\psi}(x)$, referred to as a dual wave function, can be introduced as a formal derivative of the wave function $\boldsymbol{\psi}(x)$ by considering its argument x as a continuous variable. The following definition of $\tilde{\psi}(x)$ is invariant with

respect to the choice of orientations on the linear segments:

$$\tilde{\psi}(x) = \frac{1}{k}\mathrm{div}\boldsymbol{\psi}(x) \equiv \frac{1}{k}\frac{d(\boldsymbol{\psi}(x), \boldsymbol{n}_x)}{dx}, \tag{2.9}$$

where $\boldsymbol{n}_x$ is the unit vector in the positive x direction. The normalization of the dual wave function is determined by the normalization of the wave function. The relation (2.9) and the identification of the wave function with the transition dipole distribution imply the the dual wave function is associated with the transition charge distribution.

The exciton wave function and dual exciton wave function are reduced characteristics of the excitation strength that are linearly and locally related to the transition density matrix in an infinite polymer[42]. Therefore, far from vertices, the transition dipoles and charges of repeat units are proportional to the exciton wave function and dual exciton wave function, respectively. If the deviations of the charges and dipoles of repeat units from standing waves are localized near the vertices, and the linear segments are sufficiently long, we can include all such deviations into vertex contributions. Thus, in the molecule with long linear segments it is possible to take into account all contributions to the transition dipole.

The approach described above ensures that the charge and dipole of the building block is independent of its position within the molecule and depends only on the local amplitude of the excitation. For repeat units, the excitation strength is characterized by the exciton wave function and dual exciton wave function. For a vertex of degree n, the excitation strength can generally be determined by any n amplitudes of incoming or outgoing waves in the wave function or dual wave function, because the amplitudes are related to each other with the help of Eqs. (2.4) and (2.9). We choose to use the amplitudes of incoming waves in the exciton wave function and dual exciton wave function for the transition dipole and charge, as they have the corresponding symmetries. Symmetries of repeat units and vertices determine how many parameters are necessary to describe their transition dipoles and charges.

Combining all contributions, we find the following general expression for the total tran-

sition dipole of the excited state:

$$\begin{aligned}\boldsymbol{\mu} = & \sum_{\alpha\in\mathcal{M}_1}\sum_{x_\alpha=1}^{l_\alpha}\left(q(\omega)\boldsymbol{r}_{x_\alpha}^{(\alpha)}\tilde{\psi}_\alpha(x_\alpha)+d(\omega)\boldsymbol{\psi}_\alpha(x_\alpha)\right)\\ & +\sum_{b\in\mathcal{M}_0}\sum_{\alpha\ni b}\left(q_{b\alpha}(\omega)\boldsymbol{r}_b\tilde{\psi}_{\alpha b}^{(-)}+d_{b\alpha}(\omega)\boldsymbol{\psi}_{\alpha b}^{(-)}\right), \end{aligned} \tag{2.10}$$

where we introduced energy-dependent charge coefficients $q(\omega)$ and $q_{b\alpha}(\omega)$ as well as dipole tensor parameters $d(\omega)$ and $d_{b\alpha}(\omega)$ for repeat units and vertices, respectively. $\mathcal{M}_0$ and $\mathcal{M}_1$ represent sets of molecular vertices and linear segments, respectively. The two terms in Eq. (2.10) stand for contributions of repeat units and vertices, respectively. The dipole tensor parameters represent the most general forms of linear transformations between vector wave functions and vectors of transition dipoles. The positions $\boldsymbol{r}_{x_\alpha}^{(\alpha)}$ and $\boldsymbol{r}_b$ refer to the repeat unit x_α in the segment α and the vertex b, respectively. In the following, the parameters $q(\omega)$, $d(\omega)$, $q_{b\alpha}(\omega)$, and $d_{b\alpha}(\omega)$ will collectively be referred to as dipole ES parameters.

2.2 Extraction of the transition charge and dipole parameters from quantum-chemical calculations

Within the ES approach, the transition charge and transition dipole parameters characterizing different building blocks are necessary for the calculation of the total transition dipole moment of the entire structure. In this section, we demonstrate how these dipole parameters can be retrieved from the quantum-chemical computations in conjugated molecules of moderate sizes using an example of phenylacetylene molecules.

2.2.1 Quantum-chemical computations

We consider phenylacetylene-based molecules with four types of building blocks (see Fig.2.1), including a repeat unit, a molecular terminal, and *meta*- and *ortho*-conjugated linkages. The transition charge and dipole parameters of these building blocks are retrieved from the quantum-chemical calculations performed in linear molecules as well as *meta*- and *ortho*-conjugated molecules of different lengths[43]. The ground state geometries are optimized using the semiempirical Austin Model 1 (AM1) Hamiltonian[61], which adequately

reproduces the molecular ground state geometries, particularly in π-conjugated hydrocarbon compounds[43]. Gaussian 03 package[62] is used for the ground state optimizations.

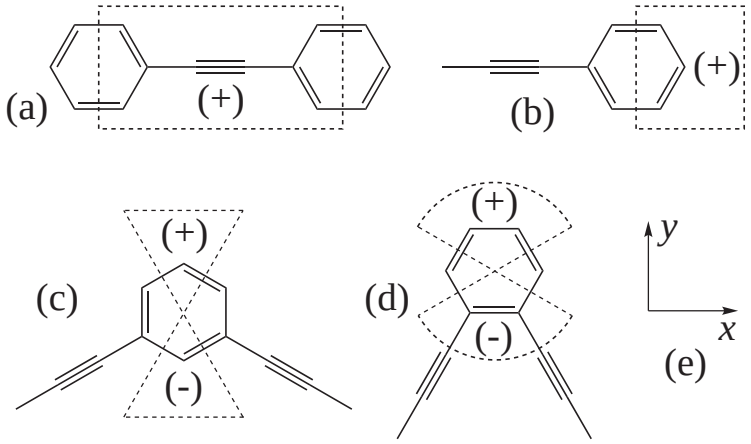

Figure 2.1: Building blocks of phenylacetylene-based molecules: (a) repeat unit, (b) molecular terminus, (c) *meta*- and (d) *ortho*-conjugated linkages (joints). The atoms in the region marked with"(+)" should be considered as part of the vertex, whereas those in the region marked with "(-)" should be "deducted" from the joint due to the overlap of the attached repeat units. (e) the coordinate system for the transition dipole in the vertices shown here.

The collective electronic oscillator (CEO)[46, 63, 64] representation is used to compute the excited states in all molecules. In this technique the Hartree-Fock (HF) ground state density matrix and the INDO/S semiempirical Hamiltonian are employed in the TDHF equation to compute the excitation energies and other molecular spectroscopic observables. The computation cost per excited state is comparable to that of the ground state[46]. The CEO approach has been successfully applied for computing the optical excitations of large conjugated molecules. The excitation energies, oscillator strengths, the transition density matrices in the molecular orbital space and atomic orbital space are obtained.

2.2.2 Transition charge and dipole ES parameters of repeat units

The transition charge $q(\omega)$ and dipole $d(\omega)$ parameters of a repeat unit are retrieved from the quantum chemistry data of linear molecules. Because the ES approach is asymptotically exact for molecules whose length is significantly larger than the exciton size[42] (2-3 repeat units in phenylacetylenes), the molecules selected for the parameter extraction should not

be too short. To obtain the parameters at low energy, the molecules should be as long as possible. We computed the first 25 to 40 excitations in molecules between 10 and 59 repeat units in length. We focus on the lowest excitonic band (2.83-4.1 eV), which appears as a strong peak in the optical absorption spectra (band-gap transition). These delocalized light excitons[43], which can be distinguished from other exciton types with the help of the transition density matrices, are chosen for the detailed analysis. To determine the dipole parameters with adequate accuracy in the large portion of the band (for the energies higher than 2.9 eV), it is sufficient to perform quantum chemistry calculations in several molecules shorter than 20 repeat units. We use several additional longer molecules to improve accuracy at the lower energies.

In these linear molecules, for each excited state in the band of light excitons corresponding to fundamental optically active excitonic band at the band-gap, we calculate the exciton wave function and dual wave function from Eqs. (2.3), (2.4), (2.5) and (2.9) with the ES parameters extracted previously[43]. Then we use the approach outlined in Section 2.1.2 to compute the transition charges $Q(x)$ and dipoles $\boldsymbol{\mu}(x)$ of repeat units from the corresponding transition density matrix. The charge parameter $q(\omega)$ can be found from the ratio $Q(x)/\tilde{\psi}(x)$ far from the molecular termini. For light excitons the transition dipoles are directed along the repeat units. Therefore, the dipole tensor of the repeat unit is proportional to the unit matrix. We can use the ratio $\mu(x)/\psi(x)$ of projections far from the molecular termini to determine its only parameter $d(\omega)$ (we use the same notation for the tensor and the value of its identical diagonal components).

At the repeat units close to the scattering centers, the profiles of the transition dipole and charge distributions deviate from the standing waves (see Fig. 2.2). In general, the deviations of the ratios $Q(x)/\tilde{\psi}(x)$ and $\mu(x)/\psi(x)$ from the constants are localized within several repeat units from the scattering center. To calculate the dipole parameters of the repeat unit, we exclude results from three repeat units adjacent to the scattering center as well as repeat units where the denominator in $Q(x)/\tilde{\psi}(x)$ or $\mu(x)/\psi(x)$ is small and take the

average over remaining repeat units. The extracted parameters for the repeat unit shown in Fig. 2.3 are smooth functions of the energy.

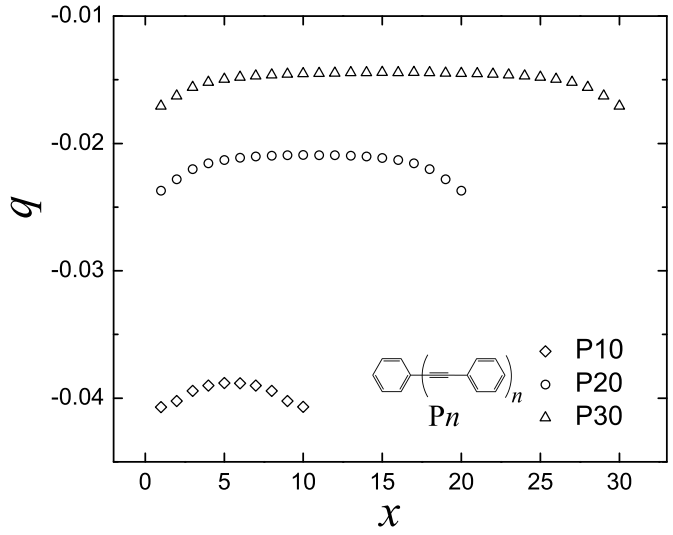

Figure 2.2: Ratios $Q(x)/\tilde{\psi}(x)$ of the repeat unit's transition charges and values of the dual exciton wave function for the first mode at all repeat units (see Fig. 1a) along linear molecules of different lengths (the molecular structure is shown in the inset).

2.2.3 Transition charge and dipole ES parameters of scattering centers

Because molecular vertices violate discrete translational symmetry of the polymer, one can expect that transition charges and dipoles of repeat units near vertices deviate from the standing-wave forms of their distributions found far from vertices. Thus, there are two types of contributions to the transition charge and dipole of a vertex: the internal contribution from all of the atoms within the vertex, and the external contribution from the transition charge and dipole deviations on the repeat units close to the vertex. The internal transition charge and dipole can be directly calculated from the transition density matrix. The deviations on the repeat unit x_α of a linear segment α can be found as

$$\Delta Q(x_\alpha) = Q(x_\alpha) - q(\omega)\tilde{\psi}_\alpha(x_\alpha), \tag{2.11}$$

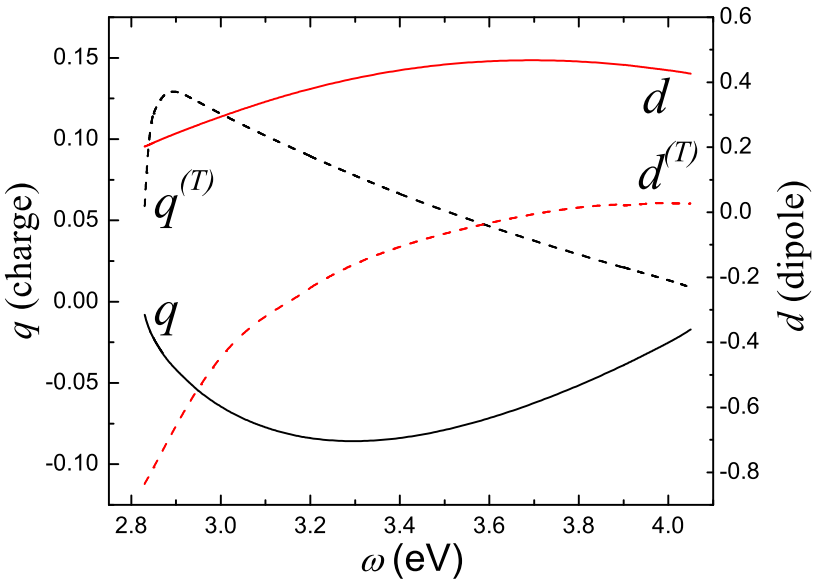

Figure 2.3: Dipole parameters q and d of the repeat units (solid lines) and real coefficients $q^{(T)}$ and $d^{(T)}$ (dashed lines) that parameterize the dipole parameters of the molecular termini (see Fig. 2.1).

$$\Delta\boldsymbol{\mu}(x_\alpha) = \boldsymbol{\mu}(x_\alpha) - d(\omega)\boldsymbol{\psi}_\alpha(x_\alpha), \tag{2.12}$$

where $Q(x_\alpha)$ and $\boldsymbol{\mu}(x_\alpha)$ are the transition charge and dipole of the repeat unit x_α. The ES parameters of repeat unit $q(\omega)$ and $d(\omega)$ have been retrieved in Section 2.2.2. Because the effect of the scattering center is typically localized within three repeat units, the external contributions can be found as sums over three adjacent repeat units in each branch attached to the vertex. The external contribution to the transition charge of the vertex b is a sum of deviations in all repeat units in attached segments α: $\Delta Q_b = \sum_{x_\alpha} \Delta Q(x_\alpha)$. In the external contribution to the transition dipole of a vertex, the transition dipole due to the transition charge corrections within the attached linear segments have to be considered in addition to the deviations of the transition dipoles: $\Delta\boldsymbol{\mu}_b = \sum_{\alpha,x_\alpha} \Delta\boldsymbol{\mu}(x_\alpha) + \sum_{\alpha,x_\alpha} (\boldsymbol{r}_{x_\alpha}^{(\alpha)} - \boldsymbol{r}_b)\Delta Q(x_\alpha)$.

The transition charge and dipole parameters of molecular termini are also extracted from the quantum chemistry data of linear molecules. The internal transition charge and dipole are attributed to the three carbon atoms and three hydrogen atoms of the terminus as shown in Fig. 2.1(b). The external contribution is from the three repeat units close to the terminus. In the transition dipole calculation [Eq. (2.10)], the ES parameters $d_{T\alpha}(\omega)$ and $q_{T\alpha}(\omega)$ of

the molecular terminus are defined with respect to the incoming waves of the exciton wave function and dual wave function, respectively. Note that the dipole parameter of the terminus is represented by a diagonal matrix whose diagonal elements are all equal. We use the same notation $d_{T\alpha}$ for both the tensor and its diagonal components. Since the incoming wave is linearly related to the full exciton wave function (which includes both incoming and outgoing waves), the latter can be used instead to define real-valued charge and dipole parameters of the terminus. Comparing its transition dipole and charge with the exciton wave function, we obtain the real-valued parameters $q^{(T)}(\omega)$ and $d^{(T)}(\omega)$ shown in Fig. 2.3. They can be used to parameterize the complex-valued dipole and charge parameters, $d_{T\alpha}$ and $q_{T\alpha}$ (which enter the general expression (2.10) for the total transition dipole and are defined with respect to incoming waves):

$$d_{T\alpha} = \left(1 + e^{i\phi_T}\right) d^{(T)}, \tag{2.13}$$

$$q_{T\alpha} = -i \left(1 + e^{i\phi_T}\right) q^{(T)}. \tag{2.14}$$

The extraction of the ES parameters of the double joints (represented by a *meta-* or *ortho*-conjugated benzene ring) requires the quantum-chemical calculations in the two-arm molecules, hereafter referred to as V-shape molecules. Several symmetric *meta-* and *ortho*-conjugated molecules of moderate size are used to retrieve the transition charge and dipole parameters for the joints.

In the benzene ring of the linkage, the part of the structure marked with "(-)" in Fig. 2.1 is counted twice due to the overlap between the joint and the attached repeat units. Therefore, the contributions of the transition charge and dipole from the overlap region should be subtracted from those from the region marked with "(+)" when computing the internal contribution of the transition charge and dipole of the joint. The transition charge and dipole deviations in the three repeat units on each side of the joint are considered as the source of the external contribution to the joint.

For the planar molecules considered, the dipoles lie in the molecular plane and can be

described by two components in the coordinate system shown in Fig. 2.1. In symmetric two-segment molecules, the excitations can be either symmetric or antisymmetric, with the symmetry being defined as the symmetry of the x projection of the transition dipole distribution. The transition charge distribution and the y projection of the transition dipole distribution have the same symmetry that is opposite to the symmetry of the x projection of the transition dipole distribution.

The number of parameters necessary for describing vertices can be generally determined from their symmetry. The transition charge and dipole of a symmetric V joint (V being meta (M) or ortho (O) joint) can be described by one and two real parameters, respectively. As it has been done for the terminals, it is more convenient to deal with real-valued parameters extracted from the transition charge and dipole distributions and afterwards relate them to the parameters that appear in Eq. (2.10).

Two charge parameters for the segments are equal, and we can use a single real parameter to express the charge through the values of the dual wave function. The real-valued charge parameters of the double joints $q^{(V)}(\omega)$ are obtained by dividing the transition charge by the sum of the values of the dual wave functions on both sides of the joint. Therefore, the transition charge parameters of a double joint, in terms of the incoming waves of the dual wave functions, can be expressed as

$$q_{V\alpha} = \left(1 + ie^{i(\phi_V + \theta_V)}\right) q^{(V)}, \tag{2.15}$$

where ϕ_V and θ_V (V stands for M or O) represent the scattering phases at the symmetric joint V which appear in the transformation between the incoming waves and full wave functions.

We observe that the transition dipoles of the double joints are directed along the x and y axes for symmetric and antisymmetric modes, respectively. This indicates that the dipole tensors $d_{V\alpha}$ associated with two segments ($\alpha = 1, 2$) attached to the double joint are equal, with x and y being their principal axes. Real-valued dipole parameters of symmetric double joints can be defined with respect to linear combinations of the exciton wave functions or dual wave functions with the proper symmetry. In particular, we define $d_x^{(O)}(\omega)$ as a real

parameter that relates the sum of projections $(\boldsymbol{\psi}_1, \boldsymbol{n}_1) + (\boldsymbol{\psi}_2, \boldsymbol{n}_2)$ onto the corresponding segments to the x component of the dipole of the *ortho* joint. Next, $d_x^{(M)}(\omega)$ relates the difference of the dual wave functions $\tilde{\psi}_1 - \tilde{\psi}_2$ to the x component of the dipole of the *meta* joint. The parameters $d_x^{(O)}(\omega)$ and $d_x^{(M)}(\omega)$ are defined differently to avoid numerical errors that would appear because of the weakness of transmission through the *meta* joint. Finally, we define $d_y^{(V)}(\omega)$ (where $V = M$ or $V = O$) in the same way for both joints as a real parameter that relates the sum of the dual wave functions $\tilde{\psi}_1 + \tilde{\psi}_2$ to the y component of the dipole. Thus, for light excitons, the dipole contribution of each symmetric double joint is determined by two real parameters, which are shown in Fig. 2.4. The complex parameters used in Eq.(2.10) are expressed through the real parameters as

$$d_{M\alpha,x} = d_x^{(M)} \left(i + e^{i(\phi_M - \theta_M)}\right) / \left(\boldsymbol{n}_\alpha, \boldsymbol{n}_x\right), \tag{2.16}$$

$$d_{O\alpha,x} = d_x^{(O)} \left(1 + ie^{i(\phi_O - \theta_O)}\right) / \left(\boldsymbol{n}_\alpha, \boldsymbol{n}_x\right), \tag{2.17}$$

$$d_{V\alpha,y} = d_y^{(V)} \left(i - e^{i(\phi_V + \theta_V)}\right) / \left(\boldsymbol{n}_\alpha, \boldsymbol{n}_y\right), \tag{2.18}$$

where the last equation represents equations for both the meta ($V = M$) and ortho ($M = O$) joints, and $\boldsymbol{n}_\alpha$, $\boldsymbol{n}_x$ and $\boldsymbol{n}_y$ are the unit vectors in directions of attached linear segments α and along x and y axes.

Geometry distortions due to steric interactions appear in planar orthoconjugated molecules. First, for the optimized planar geometry, the angle between the segments attached to the ortho joint is about 65 degrees (different from $\pi/3$). This angle, measured between triple bonds adjacent to the ortho joint, appears to be the property of the joint independent of the overall molecular structure, as we observe almost the same value in several types of molecules with different lengths of linear segments. The external contribution to the dipole parameter of the ortho joint depends on this angle. However, the dipoles of the vertices are usually much smaller than the total dipole of the molecule (our approach is asymptotically exact for long linear segments with many repeat units, whose dipoles are comparable to or larger than dipoles of vertices). More important is the orientation and position of repeat units over

the full length of the linear segments. The segments tend to be straight if their ends are not constrained, such as in two-segment ortho molecules or in zigzag molecules considered below. In fact, the direction of the triple bonds changes by less than a half degree between the ortho joint and the end of the long segment attached to the joint, with the most change happening within 2-3 repeat units from the joint. Thus, in the arms with free ends, the angle between symmetric triple bonds starts at 65 degrees for repeat units adjacent to the ortho joint and saturates at $65.73 \sim 65.75$ degrees. The situation is different if the arms are constrained as in molecules with loops including triangles and parallelograms. In the equilateral triangle, for example, the segments are bent outwards, and this distortion is not localized near the ortho joints.

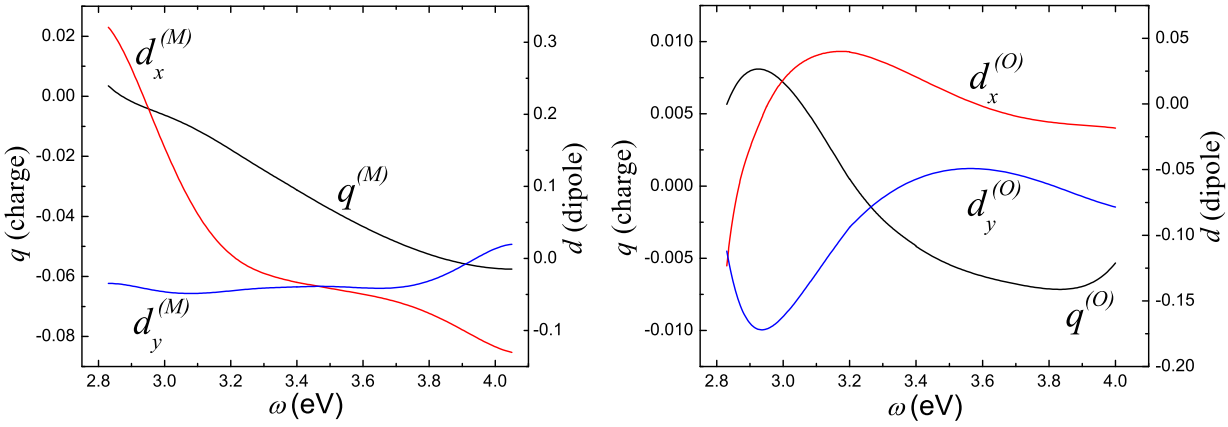

Figure 2.4: Real coefficients $q^{(V)}$, $d_x^{(V)}$ and $d_y^{(V)}$ that parameterize the dipole ES parameters of the meta ($V = M$) and ortho ($V = O$) joints.

2.3 Accuracy of the ES model for transition dipoles

We recently demonstrated[43, 44] how the ES model can be applied to compute excitation energies in branched conjugated molecules. In this section, we use the same types of molecules to test how well the dipole extension of the ES approach works that allows us to predict absorption spectra. Before the transition dipoles are calculated, the excitation energies and exciton wave functions are found by applying the energetic ES approach with the previously

extracted dispersion relation and scattering matrices.

First, in order to check the quality of the ES dipole and charge parameters for molecular ends and repeat units, we compare ES estimates calculated from Eq. (2.10) and quantum-chemical results in linear molecules. The ES approach delivers good accuracy of such calculations as shown in Fig. 2.5. Although the ES approach is asymptotically exact for long molecules [42], and the dipole parameters are extracted from the molecules longer than 10 repeat units, for short molecules the relative error of the calculation is acceptable ($< 10\%$). For molecules whose length is larger than the exciton size (>3 repeat units), the relative error is less than 5%.

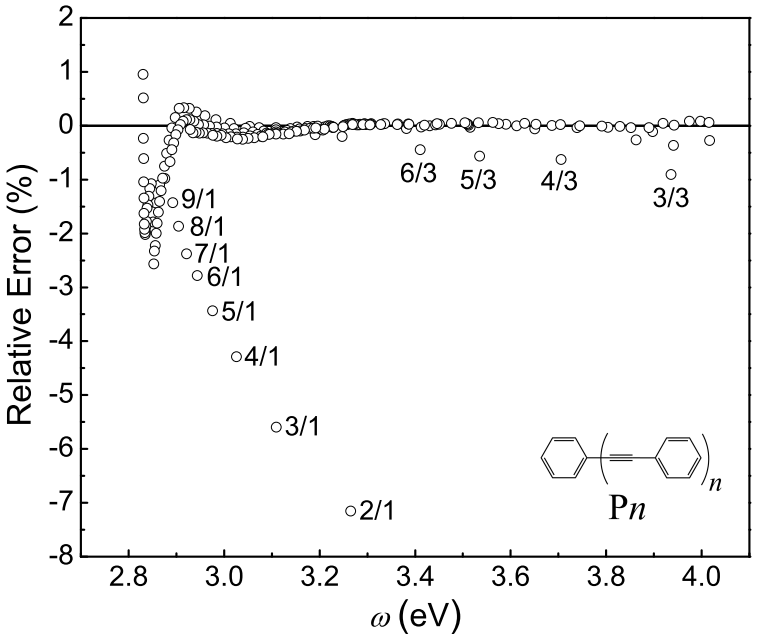

Figure 2.5: Relative deviations of the transition dipoles in linear molecules (shown in the inset) calculated using the ES approach compared to CEO computations. The mth mode in the molecule Pn is denoted by n/m.

Next, we verify the accuracy of the transition charge and dipole parameters that describe the *meta*- and *ortho*-conjugated joints by comparing the transition dipoles calculated within the ES approach and by the quantum-chemical computations in V-shape molecules. For selected molecules, the relative error of the transition dipole shown in Fig. 2.6 is calculated by comparing the ES result with that of the brightest state from the quantum chemistry

data.

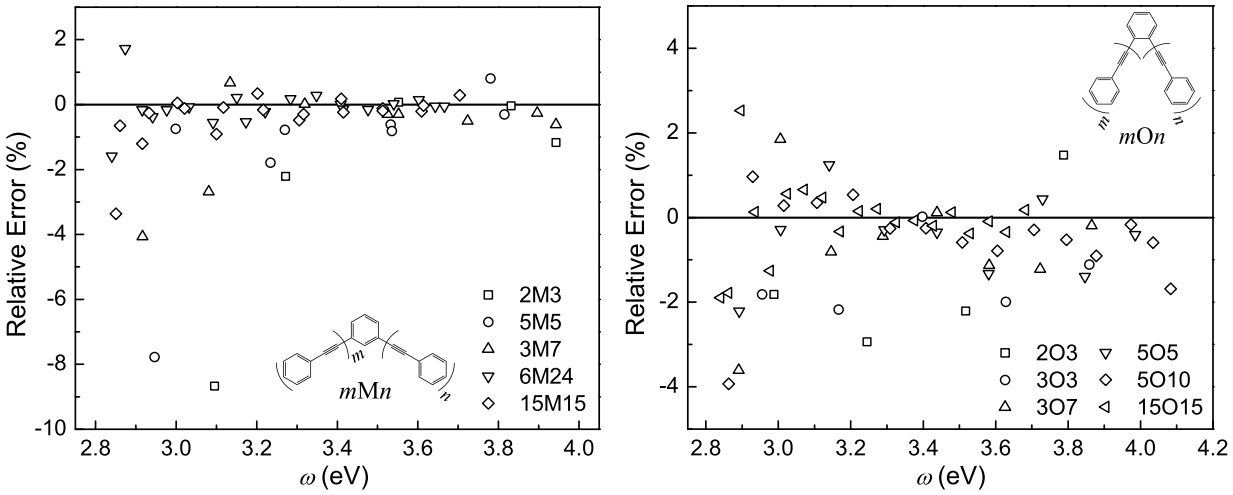

Figure 2.6: Deviations between the ES and CEO transition dipoles relative to the transition dipoles of the brightest states in *meta*- and *ortho*-conjugated molecules (shown in the insets).

In the ES calculation of transition dipoles in molecules with ortho joints, taking into account actual geometry turns out to be important. Although the linear segments connected by the ortho joint can be considered straight, the angle between them is 65.75 degrees. We use this geometry in all molecules with unconstrained ortho joints.

The scattering phases for the *meta* and *ortho* joints are close to the values that correspond to total reflection and ideal transmission, respectively[43]. Consequently, the exciton is more confined within the linear segments in a *meta*-conjugated molecule than in an *ortho*-conjugated molecule. Because stronger reflection at vertices typically leads to larger deviations of excitations from the plane-wave forms, the errors of the ES approach can be expected to be larger in short *meta*-conjugated molecules than in *ortho*-conjugated molecules of the same length. For example, we observe that the error of the brightest state (the second mode) for $2M3$ is larger than for $2O3$ (see Fig. 2.6).

At this point, we can apply the ES approach to the spectroscopic calculation in complex molecules that include the four types of building blocks shown in Fig. 2.1. As the next example we consider three-segment zigzag molecules including *meta* and/or *ortho* joints.

The notation $l_1V_1l_2V_2l_3$ for the zigzag molecules shows the order in which the vertices V_1 and V_2 connect linear segments with l_1, l_2, and l_3 repeat units. Three-segment zigzag molecules have two stereoisomers, *cis* and *trans*. Within the ES approach, the excitation energies are determined by how the building blocks are locally connected to each other, which is identical in both isomers. As a result, the ES excitation energies of the two isomers are equal. Figure 2.7 shows the transition energies and dipoles of isomers of $5O7O3$. Although the excitation distribution in the linear segments of isomers are the same, they have different transition dipoles because of different mutual orientation of the segments. For the molecule *trans*-$5O7O3$, the strongest optical transition is the third excited state, while it is the second excited state in *cis*-$5O7O3$. Compared with the quantum chemistry results, the deviation of the transition dipole calculated by ES approach is less than 6% (see Fig. 2.8).

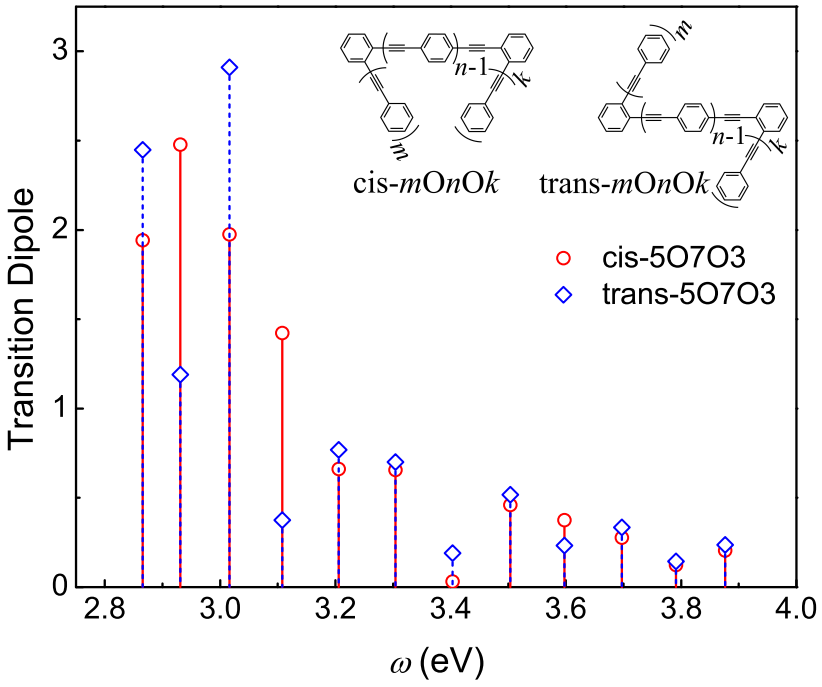

Figure 2.7: The transition dipoles of zigzag isomers (shown in the inset) computed by the ES approach. The excitation energies are identical for isomers.

For equilateral triangular molecules, we obtain similar accuracy as for zigzag molecules. Fig. 2.9 shows transition dipoles of the two triangular molecules $T6$ and $T7$ (Tn denotes the triangular molecule with the side of n repeat units) computed by using the ES approach.

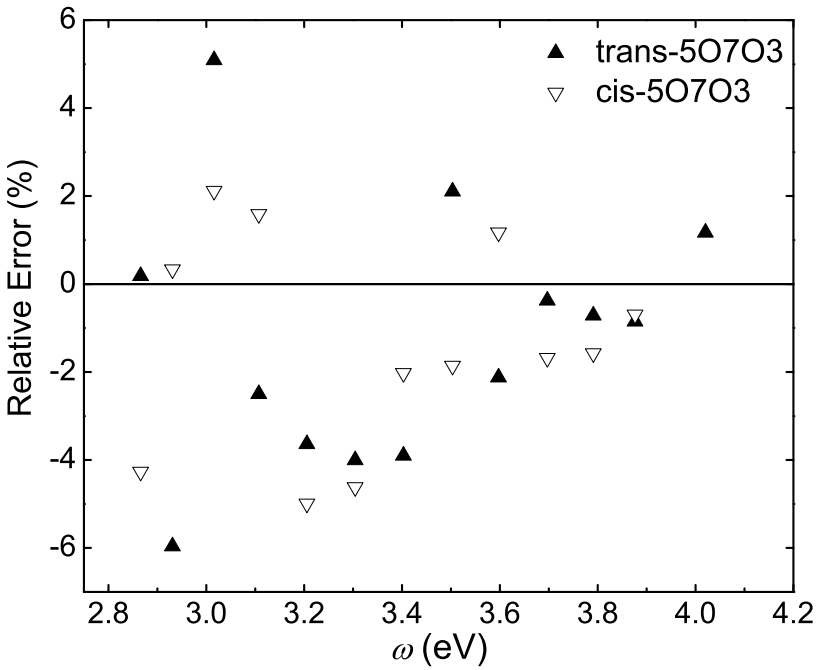

Figure 2.8: The deviations between the ES and CEO transition dipoles relative to the transition dipoles of the brightest state in zigzag isomers.

In the actual optimized geometry the segments of the triangular molecules are slightly bent outwards because the angle between them at the ortho joints is about 65 degrees. The accuracy of the transition dipole calculation is not improved if orientations and positions of repeat units are modified according to the actual geometry. Due to the symmetry, all modes in the triangular molecules can be characterized by their angular momenta $m = 0, \pm 1$[44]. For $m = 0$ states, the transition dipoles of the three sides are equal because of the rotational symmetry. As a result, in the spectrum of a triangle molecule, all such states are dark (shown with zero dipoles in Fig. 2.9), and only the doubly degenerate modes with $m = \pm 1$ are visible. The ES approach accurately reproduced the CEO results as shown in Fig. 2.10. The results for triangular molecules illustrate that the ES approach works well for the electronic excitations with energy degeneracy.

The ES approach is designed to predict the results of the quantum chemistry that is coupled to the ES model. In this regard, the ES approach complements the established quantum-chemical methods, extending their capability while avoiding the difficulties char-

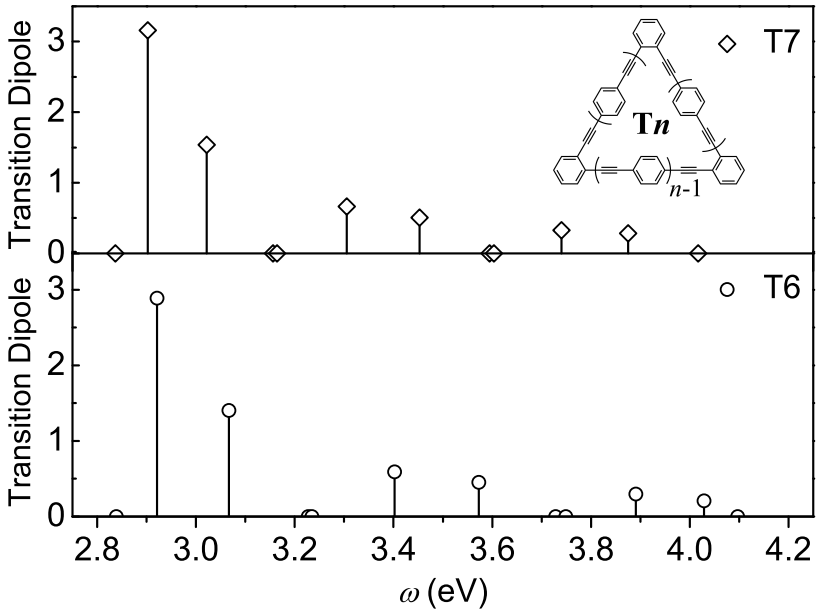

Figure 2.9: The transition dipoles of triangular molecules $T6$ and $T7$ (shown in the inset) computed by the ES approach.

acteristic of their use in large molecules with complex excitations. The transition dipole extension of the ES approach allows calculation of oscillator strengths with sufficient accuracy. Qualitative features of optical spectra of branched conjugated molecules can also be understood with the help of the ES approach. In particular, the effects of symmetry on the spectra can be easily explained within the ES approach. One can also rationalize how small modifications of the molecular geometry, which do not change excitation energies, affect the intensities of spectral peaks.

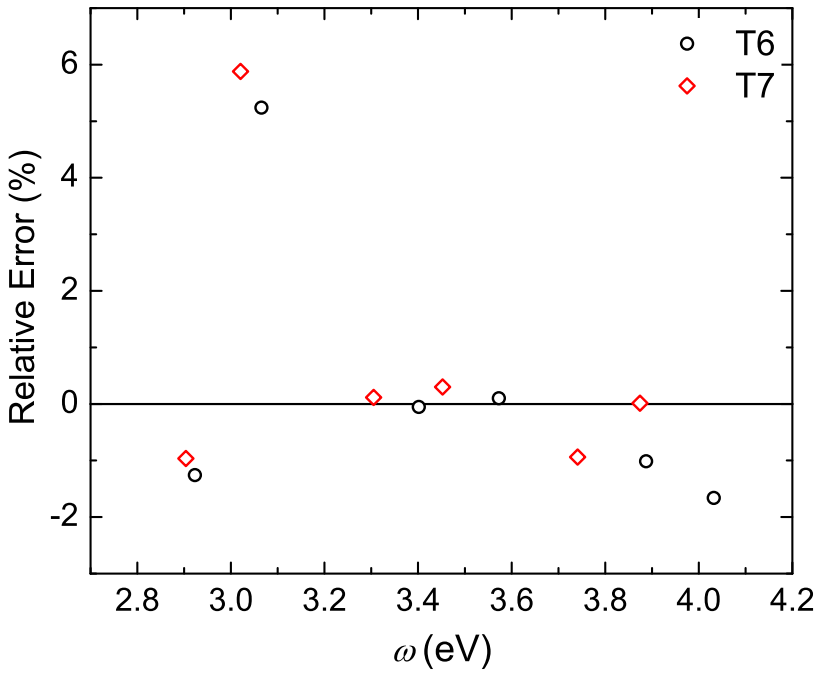

Figure 2.10: The deviation between the ES and CEO transition dipoles of doubly degenerate modes relative to the transition dipoles of the brightest state in triangular molecules $T6$ and $T7$.

Chapter 3

Electronic excitations in donor and acceptor substituted conjugated oligomers

Previously we applied the ES methodology to phenylacetylene (PA) oligomers with *ortho*- and *meta*-conjugated double joints using the time-dependent Hartree-Fock (TDHF) theory [43, 44, 65] as a reference quantum chemistry. The results of the ES approach were quite accurate. Thus far we have focused on application of the ES approach to pure hydrocarbon systems, i.e., molecules without extraneous polar moieties that could noticeably perturb the π-electron density distribution and possibly violate the electron-hole symmetry. Presence of electron-donating and/or accepting groups in conjugated systems is known to substantially modify their electronic and optical properties, which is important for various potential applications [4–7, 66–75]. For example, linear conjugated molecules with donor and acceptor end-groups can show an increase of nonlinear optical response by orders of magnitude [71, 72].

In this chapter, we illustrate the capability of the ES approach by considering phenylacetylene (PA) oligomers with several common electron donor or acceptor end-groups. Qualitatively, such polar moieties modify the terminal potential experienced by a photoexcited electron or hole. From the ES perspective, because the violation of the electron-hole symmetry is expected to be localized near the modified termini [76], they can be characterized by

the energy-dependent ES parameters—the reflection phase as well as the transition charge and dipole parameters—which uniquely identify each substituent. Consequently, these ES parameters can be used to quantify the effect of substitution on the electronic spectrum of the molecule. Further, they can be added to the library of molecular building blocks, which enables us to apply the ES approach to any system with characterized donor and acceptor moieties.

3.1 Conjugation effect and reflection phases of donor and acceptor substituted termini

As examples, we consider the molecular termini of PA oligomers with three polar substituents in *para* position: two electron acceptor (-CF_3 and -NO_2) and one donor (-NH_2) groups. To obtain the reflection phases of the modified ends from the quantum-chemical calculations, we use linear molecules with only one substitution (see inset in Fig. 3.1). The exciton reflection in such molecules is determined by two reflection phases ϕ_H and ϕ_X for the terminus without substitution (i.e., hydrogen-terminated) and with the substituent X, respectively. Excitations in the given exciton band satisfy a quantization condition that has exactly the same form as for a "particle in a box" and can be rewritten as

$$\phi_X = 2\pi n - 2kL - \phi_H, \tag{3.1}$$

where k is the wavenumber, L is the molecular length, and n is an integer. Since $k(\omega)$ and $\phi_H(\omega)$ (functions of excitation energy which describe the properties of the backbone and the neutral terminus, respectively) [43] have been extracted previously, $\phi_X(\omega)$ can be readily found from the quantum-chemical transition energies. The reflection phases of studied substituted termini have been extracted by Wu et al. [1]. Once both reflection phases at the termini as well as the wavenumber are known functions of ω, one can solve Eq. (3.1) for ω to calculate the excitation energies in the given exciton band in a linear molecule with an arbitrary length, which is the simplest application of the ES approach [1].

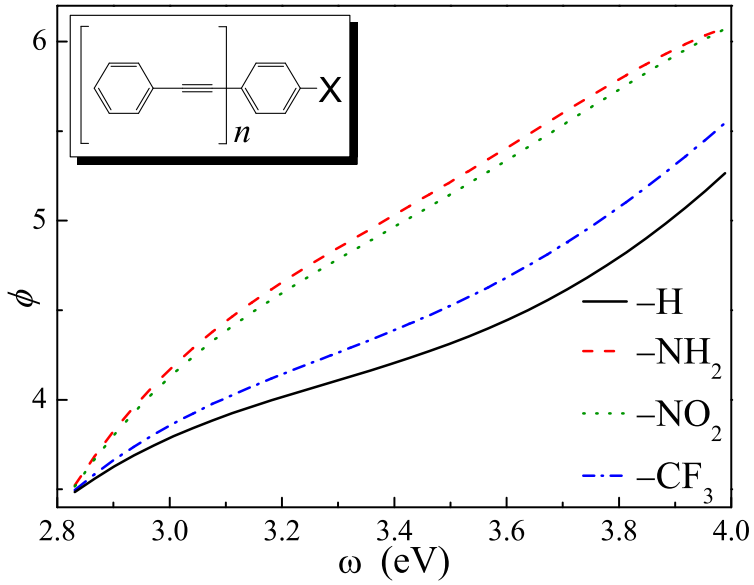

Figure 3.1: The reflection phases ϕ_X of the modified molecular termini and the reflection phase ϕ_H of the neutral (H-terminated) molecular end. Inset: linear PA oligomers with a substituent X (X= -NH_2, -NO_2 and -CF_3) on one end, which are used to extract and tabulate the reflection phases. [1]

The resulting reflection phases are shown in Fig. 3.1. As expected, the chemical structure of the substituent and its electron withdrawing/donating capacity modify the functional behavior of ϕ_X, which, in turn, alters the resulting optical spectra.

We observe that substitution decreases the excitation energies for a given oligomer length, which corresponds to the increase of the reflection phase of the terminus. It is known that any substitution with a donor or acceptor end-group extends the conjugation and increases the amplitude of the zwitterionic resonant form responsible for a partial charge transfer along the chain [77, 78], which in turn results in the red (bathochromic) shifts of the optical spectra. These phenomena can be easily quantified within the ES picture, where the excited states are associated with states of a quantum particle (exciton). The dependence of the scattering phase on the excitation energy (or wavenumber) can be understood as a measure of the conjugation length and strength. A higher value of the reflection phase ϕ_X corresponds to a longer conjugation, which implies that the exciton experiences a softer potential at the terminus.

Because of the electron-hole symmetry, one cannot deduce from the reflection phase energy dependence whether the substituent is a donor or an acceptor. Instead, the reflection phase is determined by the effective conjugation. The strong π-acceptor (-NO_2) and π-donor (-NH_2) groups similarly affect the conjugation, whereas for the weak π-acceptor (-CF_3) the reflection phase is closer to that of the unmodified end (see Fig. 3.1) [1].

The quality of the fitting functions representing the reflection phases of the donor and acceptor modified termini had been verified by applying the ES approach to several types of PA molecules [1]. The accuracy is similar to what have been observed for ES applications to unsubstituted PA molecules [43].

3.2 Calculation of the transition dipoles for donor and acceptor substituted molecules

Following the methodology developed in Ref. [65], we can also obtain the energy-dependent parameters necessary to model the transition dipole moments of the substituted oligomers. These charge and dipole parameters relate the transition charge and dipole of the terminus to the local excitation amplitudes. We emphasize that any quantitatively accurate approach for computing excited states, such as TDDFT, can be used as a reference quantum-chemical method [39]. Here we rely on the homemade collective electronic oscillator (CEO) technique [46, 63]. In principle, the electronic spectrum of only one long molecule is sufficient to obtain the ES parameters of each substituent. To get more points within the exciton band, we use a training set that consists of five linear molecules of different lengths. This allows us to confirm the main assumption of the ES approach that the exciton properties are local properties of the building blocks. For future application of the ES approach, we tabulate the new ES parameters using piecewise polynomial fitting. For a given terminus, these dipole parameters are calculated from the CEO transition density matrices between the ground and excited states in five linear molecules with the lengths varying from 15 to 30 repeat units (see inset in Fig. 3.1). In addition to the contributions of the matrix elements

corresponding to the terminal atoms, we take into account the deviations of the transition charges and dipoles of the nearby repeat units from their asymptotic standing-wave forms. The real-valued transition charge and dipole parameters of the termini are shown in Fig. 3.2. They can be used to parameterize the complex-valued dipole and charge parameters that are defined with respect to incoming waves from Eqs. (2.13). We note that the charge and dipole parameters of -NO_2 and -NH_2 substituted termini are similar because of their similar influence on π-conjugation, whereas they are quite different for a weaker acceptor -CF_3.

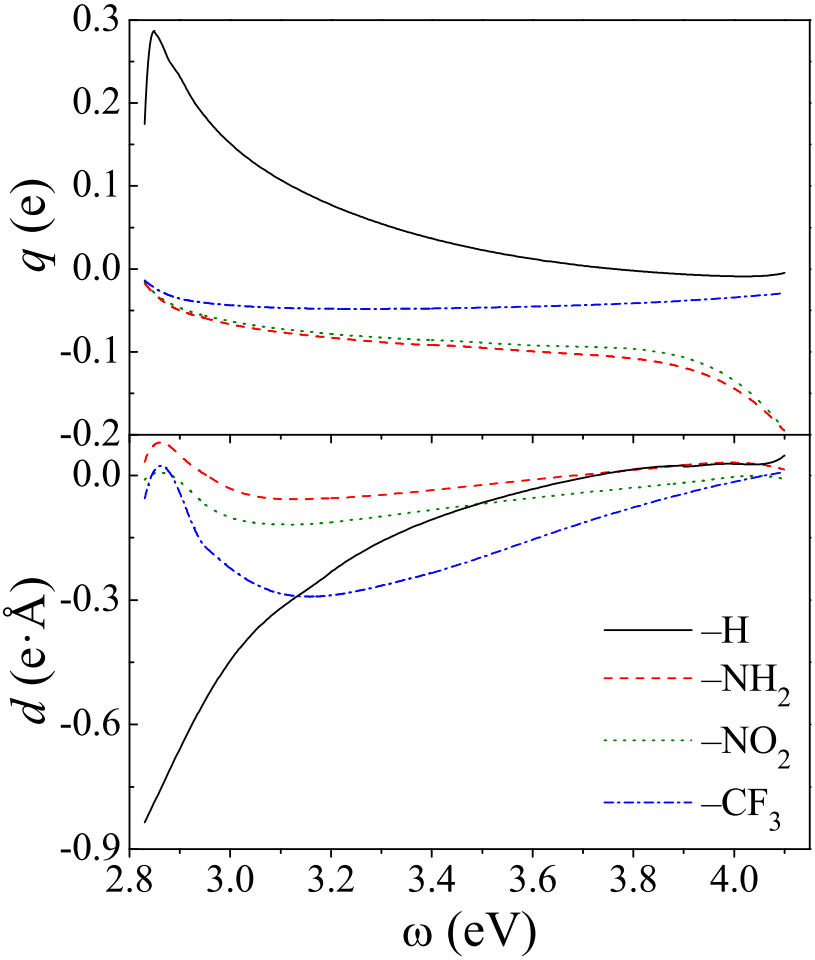

Figure 3.2: The transition charge $q^{(X)}(\omega)$ (top panel) and dipole $d^{(X)}(\omega)$ (bottom panel) parameters of donor/acceptor modified (-NH_2, -NO_2 and -CF_3) and neutral (-H) termini.

Together with the reflection phases, the transition charge and dipole parameters of the donor and acceptor substituted termini can be used within the ES approach to calculate

the absorption spectrum of any PA compound including these modified termini. We show a comparison of the ES and CEO absorption spectra for three molecules in Fig. 3.3. The relative differences of the ES and CEO transition dipoles with respect to that of the brightest state in the given molecule are less than 5% (see Fig. 3.4).

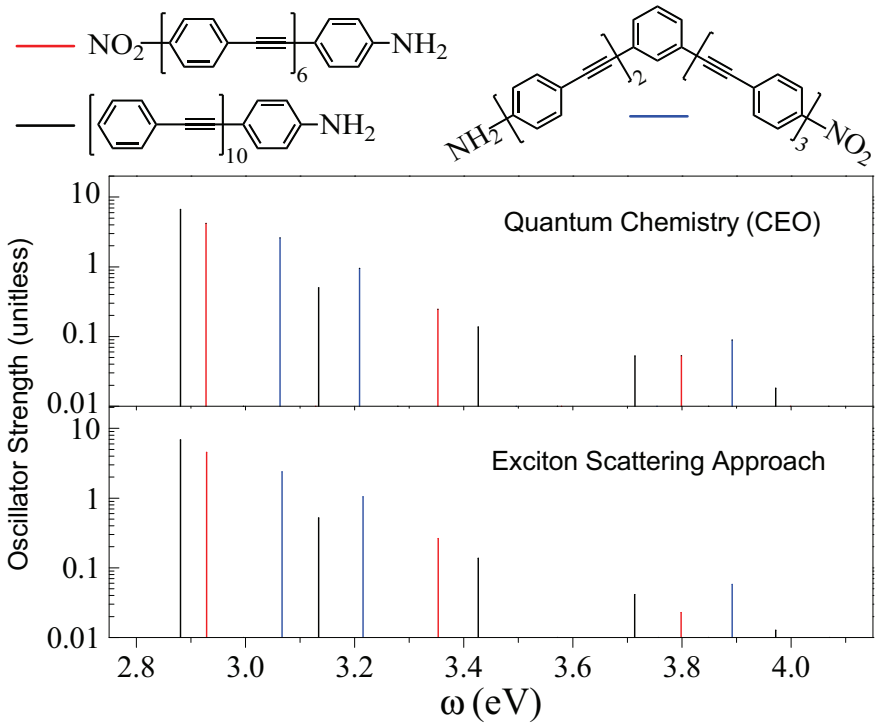

Figure 3.3: Accuracy of the ES method: comparison of optical spectra obtained with the CEO quantum-chemical technique (top panel) and the ES approach (bottom panel) for selected molecules.

Thus far, the effects of chemical substitutions with donor and acceptor moieties can be naturally incorporated into the Exciton Scattering (ES) framework designed for multiscale modeling of excited state structure and spectroscopy of large conjugated molecular systems [39]. From the perspective of the ES approach, these chemical modifications modify the reflection phases and dipole parameters of molecular termini. Thus, the donor or acceptor ability of a substituent is uniquely imprinted in the functional form of the energy-dependent ES parameters that characterize the particular group. Within the ES approach, these newly characterized termini are merely additional molecular building blocks whose scattering pa-

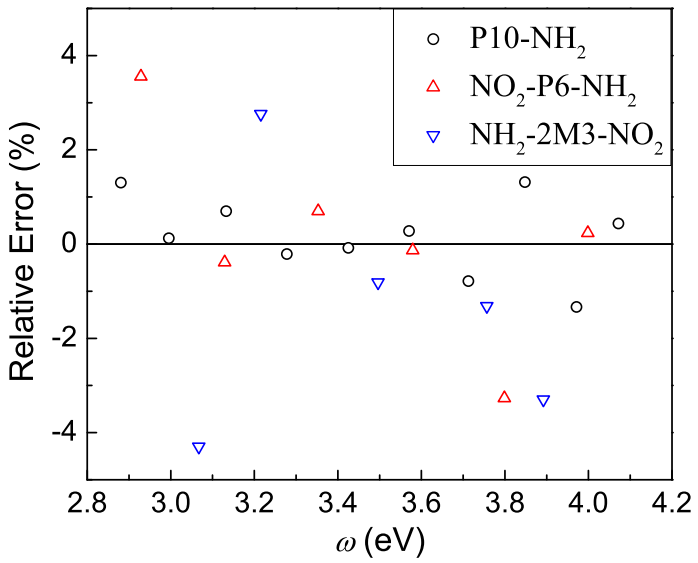

Figure 3.4: Deviations between the ES and CEO transition dipoles relative to the transition dipoles of the brightest states in donor and/or acceptor terminated molecules (structures are shown in the insets of Fig. 3.3).

rameters, combined with those previously extracted [39, 43, 65], can be used to treat a wide variety of molecules with such substitutions.

The accuracy of the ES methodology for donor and acceptor substituted molecules is similar to that previously observed for unmodified oligomers, namely a few meV for transition energies and a few percent for transition dipole moments. Thus, the ES approach accurately reproduces the reference quantum chemical calculations at a greatly reduced numerical cost, which marks its usefulness for computing electronic spectra of giant molecular systems and/or combinatorial "click chemistry" studies to achieve desired photophysical properties of organic conjugated compounds.

Chapter 4

Exciton scattering on symmetric branching centers in conjugated molecules

4.1 Library of molecular building blocks

A wide variety of chemical groups can be used as molecular building blocks to construct conjugated systems [4–7, 79]. Therefore, exhaustive search of molecular structures with desirable electronic and optical properties is time-consuming. The ES approach enables efficient computation of the excited state properties of any molecule formed by any combination of molecular building blocks from the library. Thus, the ES approach can provide a low-cost analysis of the structures, initially constructed by chemical intuition, before the real expensive synthesis and characterization take place.

In the synthesized PA-based molecules [5, 7, 8, 49], one can find only a short list of molecular vertices (see Fig. 4.1; vertices (a), (b) and (c) have been studied within the ES approach). Naturally, one direction of our work is to characterize the remaining PA joints. In this chapter we extend the capability of the ES approach by retrieving the 2×2, 3×3 and 4×4 frequency-dependent scattering matrices that describe symmetric double, triple and quadruple joints, respectively referred to as V-, Y- and X-joints (see Fig. 4.1 (b), (c), (d) and (g)). The triple joint is a common building block of dendrimeric stars (nanostars) [8]. Besides, complex molecular networks [2, 3, 6, 11] can be formed by combining previously

characterized vertices with these two joints. This allows us to extend the ES methodology to a much broader variety of branched conjugated molecules and molecular networks that consist of the characterized building blocks. We also present initial studies of the analytical properties of the scattering matrices $\Gamma(\omega)$ and, in particular, relate some simple topological invariants, associated with $\Gamma(\omega)$, to the number of electronic excitations in the conjugated molecules that contain the corresponding joints.

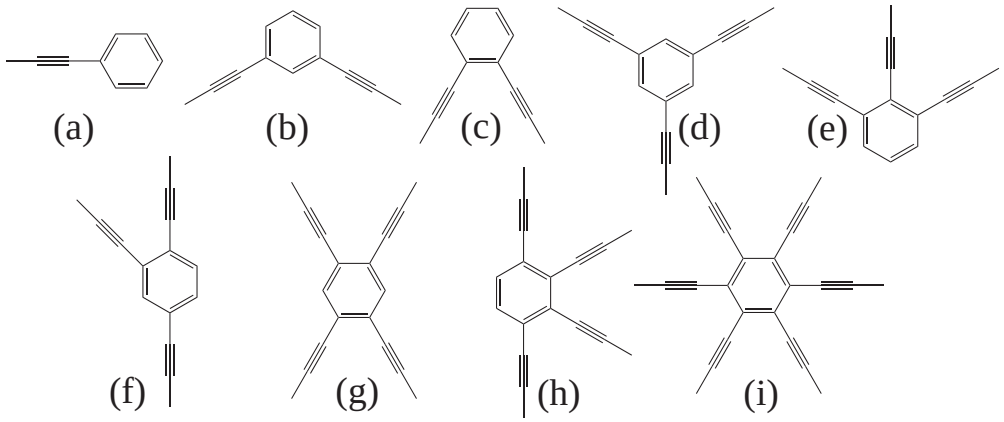

Figure 4.1: Possible phenylacetylene (PA) vertices.

4.2 Retrieving the scattering matrices for V-, Y- and X-joints

In this section we describe how the scattering matrices $\Gamma_V(\omega)$, $\Gamma_Y(\omega)$ and $\Gamma_X(\omega)$ for the double V-, triple Y- and quadruple X-joints, respectively, can be retrieved using quantum-chemical computations in molecules of moderate sizes. The scattering matrices, associated with the double, triple and quadruple joints have dimensions of 2×2, 3×3 and 4×4, respectively. Fortunately, we can take advantage of the high degree of symmetry of these joints (it is the reason why they are referred to as symmetric joints) to simplify the matrix parametrization. As shown below, due to their symmetry, the symmetric molecules can be viewed as effective linear chains, and the same computational procedure as for linear and two-arm molecules [39, 43, 80] can be employed to extract the scattering matrix elements.

4.2.1 Symmetry analysis

The scattering matrix $\Gamma(\omega)$, associated with a degree-n vertex represents a unitary linear transformation from the space $V^{(-)}$ of incoming to the space $V^{(+)}$ of outgoing waves at frequency ω, the latter standing for the excitation energy. Generally, planar vertices can remain invariant with respect to certain rotations and reflections that generate the vertex symmetry group G. Elements $g \in G$ of the symmetry group are naturally represented in the spaces $V^{(\pm)}$ by unitary operators $T(g)$, so that they act in the space of scattering matrices as $\Gamma \mapsto T(g)^{-1}\Gamma T(g)$. In the following we will use group representation theory [81] to parameterize the scattering matrices.

First we consider the symmetric V-joints, which have been studied in terms of scattering probabilities $\theta(\omega)$ and phases $\phi(\omega)$ [43]. According to the mirror symmetry the 2×2 scattering matrix has been parametrized by

$$\Gamma_V^{(2)}(\omega) = \begin{pmatrix} r & t \\ t & r \end{pmatrix} = \begin{pmatrix} \sin\theta \exp(i\phi) & i\cos\theta \exp(i\phi) \\ i\cos\theta \exp(i\phi) & \sin\theta \exp(i\phi) \end{pmatrix}. \tag{4.1}$$

The symmetry group of the V-joint is the abelian group $G_V = C_{2v}$ with four elements. The unitarity of the scattering matrix Γ_V indicates two one-dimensional irreducible representations: symmetric and antisymmetric configurations hereafter denoted as A and B respectively. Then, the unitary of the scattering matrix Γ_V can be diagonalized in an ω-independent basis:

$$\Gamma_V^{(2)} = UDU^\dagger, \;\; U = \frac{1}{\sqrt{2}} \begin{pmatrix} 1 & 1 \\ 1 & -1 \end{pmatrix}, \;\; D = \begin{pmatrix} e^{i\phi_0} & 0 \\ 0 & e^{i\phi_1} \end{pmatrix}. \tag{4.2}$$

In each representation, the scattering matrix acts as a reflection amplitude with the unit absolute value. Therefore, $\Gamma_V(\omega)$ can be parameterized by only two real energy-dependent scattering phases $\phi_0(\omega)$ and $\phi_1(\omega)$. The complex reflection and transmission amplitudes of V-joint can be represented by:

$$r = \frac{1}{2}\left(e^{i\phi_0} + e^{i\phi_1}\right), \; t = \frac{1}{2}\left(e^{i\phi_0} - e^{i\phi_1}\right). \tag{4.3}$$

The scattering matrices of symmetric triple and quadruple joints have been preliminarily studied in Wu's work [1]. In this chapter, we reformulate the scattering matrices and refine the scattering phases. New features have been observed and investigated.

For a symmetric Y-joint, its symmetry group $G_Y = D_3$ (a dihedral non-abelian group with six elements including the rotations by $\pm 2\pi/3$ and three reflections) determines a form of the associated scattering matrix

$$\Gamma_Y^{(3)}(\omega) = \begin{pmatrix} r & t & t \\ t & r & t \\ t & t & r \end{pmatrix}, \tag{4.4}$$

with $r(\omega)$ and $t(\omega)$ being complex numbers that represent the reflection and transmission amplitudes, respectively. The unitarity of the scattering matrix Γ_Y imposes two independent (real) conditions on r and t, allowing Γ_Y to be parameterized by two real parameters. Indeed, the group D_3 has two irreducible representations: a one-dimensional trivial representation and a two-dimensional representation. The former corresponds to the symmetric incoming and outgoing waves, or, in other words, the zero angular momentum, $m = 0$. The space of the second representation is spanned by two angular harmonics with $m = \pm 1$, interchanged by reflections. Therefore, the matrix Γ_Y can be diagonalized in an ω-independent basis:

$$\Gamma_Y^{(3)} = UDU^\dagger , \tag{4.5}$$

$$U = \frac{1}{\sqrt{3}} \begin{pmatrix} 1 & 1 & 1 \\ 1 & \exp(2\pi i/3) & \exp(-2\pi i/3) \\ 1 & \exp(-2\pi i/3) & \exp(2\pi i/3) \end{pmatrix},$$

$$D = \begin{pmatrix} \exp(i\phi_S) & 0 & 0 \\ 0 & \exp(i\phi_P) & 0 \\ 0 & 0 & \exp(i\phi_P) \end{pmatrix}.$$

$\Gamma_Y(\omega)$ is parameterized by only two real energy-dependent scattering phases $\phi_S(\omega)$ and $\phi_P(\omega)$. As follows from Eq. (4.4), the matrix elements of Γ_Y are related to the scattering

phases by

$$\begin{aligned} r &= \frac{1}{3}\left(\exp(i\phi_S) + 2\exp(i\phi_P)\right), \\ t &= \frac{1}{3}\left(\exp(i\phi_S) - \exp(i\phi_P)\right). \end{aligned} \tag{4.6}$$

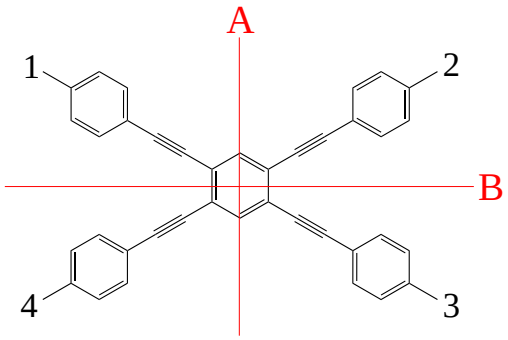

Figure 4.2: The symmetric quadruple joint (X-joint). The arm order $(1, 2, 3, 4)$ and the symmetry axes (A and B) are defined.

The symmetry group of the X-joint is the abelian group $G_X = D_2$ of order four generated by two reflections (symmetry axes A and B in Fig. 4.2) which has four one-dimensional irreducible representations. Therefore, the 4×4 scattering matrix Γ_X of the X-joint can be parameterized by four real phases ϕ_{ab} corresponding to four symmetries $A^a B^b$ where a and b can assume values 0 and 1 for the symmetric and antisymmetric configurations, or, equivalently even and odd parity, respectively. Thus, the matrix $\Gamma_X(\omega)$ can be also diagonalized in an ω-independent basis:

$$\Gamma_X = U D U^\dagger , \tag{4.7}$$

$$U = \frac{1}{2}\begin{pmatrix} 1 & 1 & 1 & 1 \\ 1 & 1 & -1 & -1 \\ 1 & -1 & -1 & 1 \\ 1 & -1 & 1 & -1 \end{pmatrix},$$

$$D = \begin{pmatrix} \exp(i\phi_{00}) & 0 & 0 & 0 \\ 0 & \exp(i\phi_{01}) & 0 & 0 \\ 0 & 0 & \exp(i\phi_{10}) & 0 \\ 0 & 0 & 0 & \exp(i\phi_{11}) \end{pmatrix}.$$

Similar to the symmetric triple joint, each energy-dependent scattering phase represents the reflection phase of an effective terminus that fully describes the X-joint for excitations of a particular symmetry. The four scattering phases $\phi_{ab}(\omega)$ are generally different without additional symmetries.

4.2.2 Numerical procedure

The numerical procedure for retrieving the scattering phases of the symmetric double, triple and quadruple joints from quantum-chemical computations is substantially simplified if we consider only symmetric (equal-arm) molecules with a V-, Y- or X-joint, i.e., the molecules that preserve the symmetry of the corresponding joint. In such molecules the excited states can be classified according to the irreducible representations of the vertex symmetry groups G_V, G_Y and G_X, respectively. In other words, the incoming and outgoing wave amplitudes form eigenvectors of the scattering matrices.

The parameterizations of the scattering matrices, presented above [Eqs. (4.2), (4.5) and (4.7)], suggest the following approach to obtain the scattering phases. For a symmetric molecule with the arms of identical length L we compute all excitation energies and transition density matrices for a given exciton type. For a certain symmetry of the excited state (determined from its transition density matrix), the scattering at the symmetric joint is equivalent to the terminal scattering for the corresponding effective linear-segment model. Consequently, the value of the corresponding scattering phase $\phi(\omega)$ (which is any of the phases ϕ_A, ϕ_B, ϕ_S, ϕ_P, ϕ_{00}, ϕ_{01}, ϕ_{10}, and ϕ_{11}) at the excitation energy ω can be found from the quantization relation

$$\phi = 2\pi n - 2kL - \phi_T\,, \tag{4.8}$$

where n is an integer, whereas the values of the wavenumber k and the phase ϕ_T of the chain terminus are found from the functions $k = k(\omega)$ and $\phi_T = \phi_T(\omega)$ tabulated previously. In principle, one can use a dense electronic spectrum of only one sufficiently large molecule to determine all features of all energy-dependent scattering phases of the Y- or X-joint. However, in the CEO computations, where the numerical cost to find all $O(N)$ excitons in the band grows as $O(N^4)$ with the number of electrons N in the molecule, the cost per a single excitation grows as $O(N^3)$. Thus, using several smaller molecules usually leads to a more efficient extraction of the ES parameters, which remains sufficiently accurate as long as the linear segments are long enough to avoid nonlocal influence of the molecular vertices. In addition, using several molecular sizes to obtain the scattering phases gives us an idea about the extent and strength of these nonlocal effects.

The quantum-chemical results for symmetric V-molecules with the arm length from 3 to 21 repeat units have been prepared for data analysis. We used symmetric Y- and X-molecules with the arm lengths from 5 to 13 and from 4 to 13 repeat units, respectively. First, we optimized the ground state geometries at the AM1 level in Gaussian03 package [62]. Then for each molecule we applied the Collective Electronic Oscillator (CEO) method [46, 63], based on the time-dependent Hartree-Fock (TDHF) theory combined with the semiempirical INDO/S (intermediate neglect of differential overlap parameterized for spectroscopy) Hamiltonian [82], to compute the vertical transition energies, transition dipoles, and transition density matrices for the first 40 excitations. By checking the transition density matrices, we selected the lowest-energy exciton band [43] as we investigated in previous chapters; the excitations were further divided into the sets according to their symmetries. Finally, each scattering phase was calculated by using Eq. (4.8).

The QC reference method should adequately describe exciton properties including the binding energy and the exciton size; the value of the latter determines how accurately the ES approach is expected to work in molecules with shorter linear segments. These exciton properties strongly depend on the amount of the Hartree-Fock orbital exchange in the density

functional [15, 83]. For example, TDDFT based on the B3LYP functional with 20% of orbital exchange results in an exciton size that is much too large and small binding energy; moreover, it is prone to the charge transfer problem [84]. Consequently, one currently prefers to use a functional with a modest amount of HF exchange (e.g., BHandH with 50% of orbital exchange) or an asymptotically corrected functional (e.g., CAM-B3LYP or LC functionals). The TDHF method based on an ab initio basis set overbinds excitons and results in a very small exciton size. On the other hand, the TDHF or CIS approaches based on the semiempirical methods can effectively reproduce excitonic properties in conjugated polymers (a detailed investigation on this topic has been performed in Ref. [85]). Therefore, we believe that our reference QC based on the semiempirical CEO method is adequate.

4.2.3 Frequency dependence of the scattering phases

The scattering phases of the *ortho*- and *meta*-joints are shown together with the reflection phase of molecular terminus in Fig. 4.3. The scattering phases of the Y- and X-joints are shown in Figs. 4.4 and 4.5 as functions of energy. The two scattering phases of the Y-joint are similar to the phases of the *meta*-joint (see Fig. 4.3). These similarities have intuitive interpretation in terms of well-known trends in organic chemistry: *meta*-conjugation at phenyl rings forms a serious obstacle for charge transfer, whereas charge is easily transferred through the *ortho*- and *para*- connections. The described property has clear signatures in chemical reactivity. It was argued in the context of experimentally obtained optical spectra in phenylacetylene dendrimers [8] that the above charge transfer properties can be extended to interpret optical properties of branched conjugated molecules. It was later shown theoretically [64] that optical excitations in branched molecules do not involve charge transfer through *meta*-connections, and can be coupled only via the coherent energy transfer mechanism. Within the ES approach, scattering at the joints that involve *meta*-conjugation only is attributed to effects of direct Coulomb interaction between the photoinduced charge densities on the connected segments [36, 43]. Therefore, the scattering phases that describe

the double *meta*-joint and the triple Y-joint, both containing *meta*-connections only, show similar frequency dependence for the corresponding symmetries.

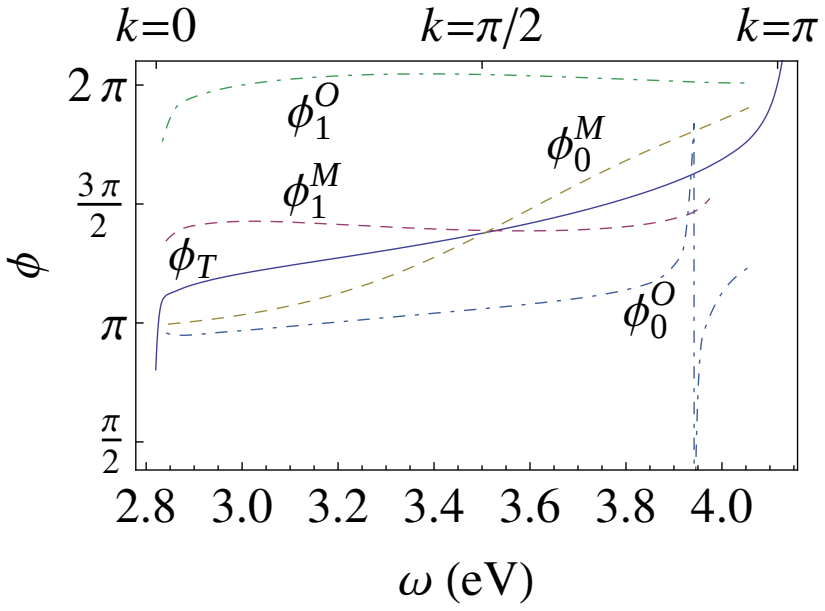

Figure 4.3: The scattering phases of the *meta(M)*- and *ortho(O)*-joints and the terminus. The scattering phases $\phi_{0,1}^M$ and $\phi_{0,1}^O$ of the double joints are defined according to the symmetry, similarly to the phases of the X-joint in section 4.2.1.

The behavior of the scattering phases of the X-joint, which has all three connections– *ortho*, *meta*, and *para*– is different from that of the Y-joint. In particular, we observe a resonance-type behavior for one of the scattering phases (corresponding to the symmetry A^1B^0) in the form of an almost-2π-kink. As shown in Fig. 4.6, the feature cannot be dismissed as resulting from the outlying points, since several molecules of different sizes contribute to the resonance shape in the phase. A similar feature is also observed for the scattering phase ϕ_0^{ortho} (corresponding to the symmetric modes in *ortho*-molecules). The other two phases associated with the X-joint, also possess a remarkable property: ϕ_{00} and ϕ_{01} seem to decrease by 2π when k changes across the Brillouin zone. All of these features will be analyzed in section 4.3.2 in terms of the topological properties of the scattering phases.

The accuracy of the retrieved scattering phases has been evaluated by applying the ES approach to several test molecules with the V-, Y- and X- joints and comparing the results

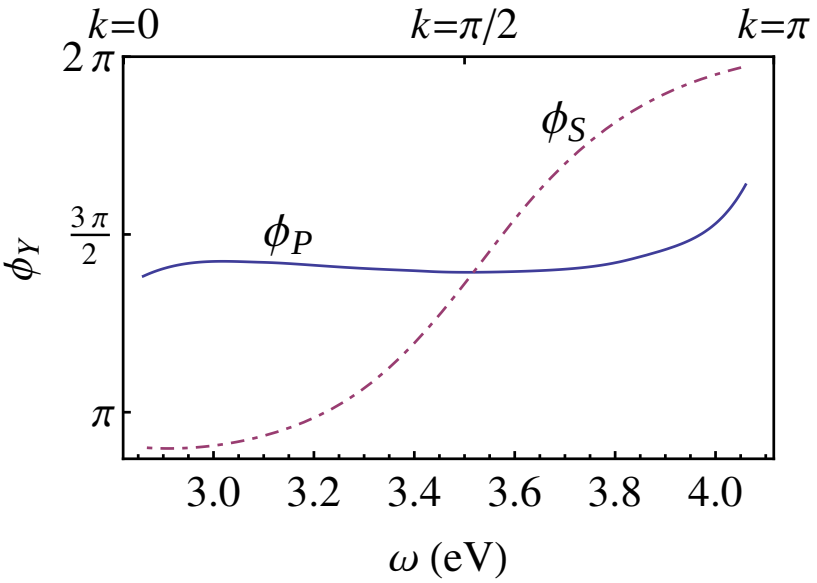

Figure 4.4: The scattering phases of the Y-joint.

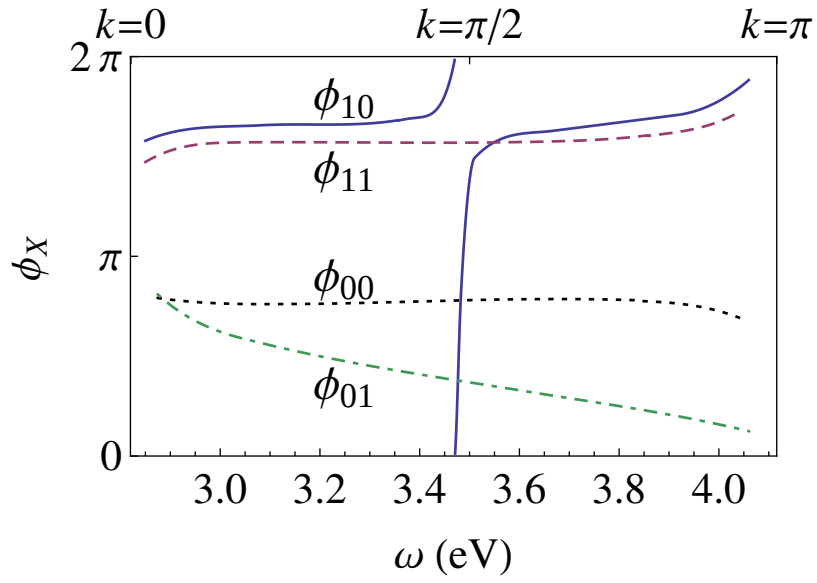

Figure 4.5: The scattering phases of the X-joint.

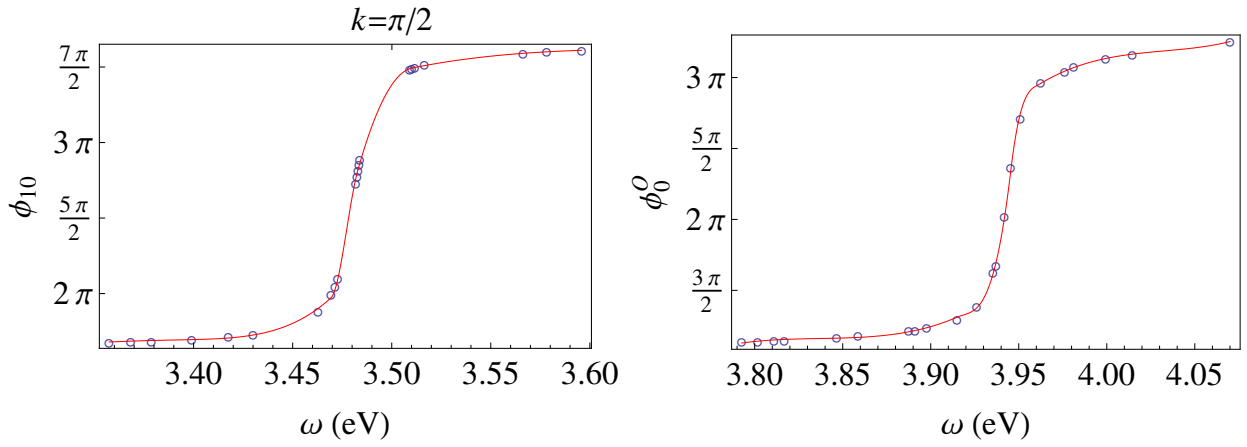

Figure 4.6: Phase ϕ_{10} of the X-joint and phase ϕ_0 of the *ortho*-joint in the vicinity of the kinks. Data points used for fitting are shown together with the fitting curve.

with the quantum chemistry computations for the corresponding test molecules, using the same reference quantum chemistry method (in this study, CEO) as was used for obtaining the ES parameters [1]. The agreement between the ES approach and the reference quantum-chemical computations is quite impressive, and the deviations are similar to those for simpler test molecules.

4.3 Topological properties of scattering phases and their physical interpretation

As mentioned in subsection 4.2.3, the frequency dependence of the phases parameterizing the scattering matrix $\Gamma_X(\omega)$ of the X-joint has very interesting qualitative features, which are unlike the behavior of the phases of all other studied PA vertices. In this section we present an initial analysis of the analytical properties of the scattering matrices describing symmetric joints, identify simple topological invariants, associated with the frequency dependence of the corresponding phases, and determine the physical meaning of the aforementioned qualitative features in terms of the invariants.

4.3.1 Analytical properties of the scattering phases and topological invariants

This subsection has two goals: (i) to introduce a set of integer-valued topological invariants, referred to as the *scattering degrees* of a vertex (one per each independent scattering phase), for a symmetric branching center, and (ii) relate the scattering degrees to the total number of excitations in a given exciton band in a molecule that consists of the symmetric branching center attached linear backbone segments of the same length.

We start with analyzing the analytical properties of the scattering matrices $\Gamma(\omega)$ that describe symmetric joints in terms of the topological invariants of the corresponding phases.

As discussed in subsection 4.2.1, scattering at the symmetric vertices is factorized according to irreducible representations of the corresponding symmetry groups. Each phase can be interpreted as the reflection phase at a terminus of some effective linear chain, and thus the scattering matrix can be efficiently analyzed in these much simpler terms.

The reflection amplitude $r(\omega) = e^{i\phi(\omega)}$ at a terminus of a linear chain is defined as the ratio of the outgoing and incoming waves amplitudes. To identify the topological properties of the scattering amplitude, we will consider it as a function $r(k)$ of the exciton momentum, related to the frequency via the exciton spectrum $\omega = \omega(k)$, rather than the frequency itself. Within the ES picture the wave function of an exciton, with the energy $\omega = \omega(k) = \omega(-k)$, on a finite segment or semi-infinite linear chain, is a superposition of two plane waves with the momenta $\pm k$

$$\psi(y) = e^{-ik(y-x)} + r_x(k)e^{ik(y-x)}, \tag{4.9}$$

where y is an integer coordinate of a repeat unit, and x is a reference point that can be chosen arbitrarily. Note that due to the time-reversal symmetry of all systems under consideration, in addition to $\omega(k) = \omega(-k)$, Eq. (4.9) implies $r(-k) = r^{-1}(k)$. Naturally, the reflection phase depends in a prescribed way on a particular choice of the reference point x:

$$r_x(k) = r_0(k)e^{2ikx}, \tag{4.10}$$

and if the reference point x is chosen, the scattering phase is well defined. Therefore, a notation $r(k)$ means that the reference point is fixed in some way.

To identify a relevant topological invariant we start with noting that, since the translational symmetry of our problem is discrete, i.e, $y, x \in \mathbb{Z}$ in Eqs. (4.9) and (4.10), the exciton momentum (strictly speaking, quasimomentum) is defined in a 1D Brillouin zone, say, $0 \leq k \leq 2\pi$, with the points $k = 0$ and $k = 2\pi$ being equivalent. Therefore, introducing a new variable $z = e^{ik}$ makes sense, and the quasimomentum can be treated as residing in a unit circle $|z| = 1$ in a complex plain $\mathbb{C}$. By its definition the scattering amplitude $r = e^{i\phi}$ also resides in a unit circle $|r| = 1$ of the complex plain.

Therefore, the scattering phase, as a function $\phi(\omega)$ of the exciton frequency, or, equivalently, as a function $\phi(k)$ of the exciton momentum, can be viewed as $r(z)$, i.e., a map $S^1 \to S^1$ of a circle $|z| = 1$ to a circle $|r| = 1$. Such a map has a simple and very natural integer topological invariant $m \in \mathbb{Z}$, referred to as the *degree* of the map [86], that represents the number of times $r(z) = e^{i\phi(k)}$ winds over the circle, while $z = e^{ik}$ goes once over the Brillouin zone. This winding number can be represented as

$$m = \int_0^{2\pi} \frac{dk}{2\pi} \frac{d\phi(k)}{dk} \tag{4.11}$$

$$= \oint_{|z|=1} \frac{dz}{2\pi i} r^{-1}(z) \frac{dr(z)}{dz}. \tag{4.12}$$

Summarizing, we have associated with any terminus a topological invariant m_x, referred to as the *degree of the terminus* (or the corresponding scattering phase), defined by Eq. (4.12) in terms of the scattering amplitude $r_x(z)$, which depends in a prescribed way on a particular choice of the reference point (i.e., m_x changes by 2, when x changes by 1). Note that due to the latter property [which immediately follows from Eq. (4.10)] the position of the reference point x, that was initially restricted to integer values, can be extended also to half-integers, if the latter choice makes the formalism more convenient.

The half-integer choice of x turns out to be convenient for the considered case of PA oligomers: we define the scattering amplitude at positions $x = 1/2$ on the linear segments

(shifted by $-1/2$ from the first repeat unit of the segment, when counted from the vertex) to obtain a simple relation between the outgoing wave on one end of the segment and the incoming wave on its other end [Eq. (2.3)], which leads to a quantization condition in the form of Eq. (4.8).

Having introduced the scattering degrees associated with the relevant vertices, which accomplishes the goal (i), we are now in a position to achieve the goal (ii), described at the very beginning of this subsection. To that end we start with noting that in a linear segment of length L (measured in repeat units) with two termini A and B described by the reflection phases $\phi_A(k)$ and $\phi_B(k)$, the quantization condition

$$2kL + \phi_A(k) + \phi_B(k) = 2\pi q, \tag{4.13}$$

is satisfied with an integer q for a state that consists of two plane waves with the wavenumbers $\pm k$. Therefore, the solutions of Eq. (4.13) that are labeled by the opposite values of k correspond to the same physical state, and, counting the solutions of Eq. (4.13), we count each physical state twice.

To count the solutions of Eq. (4.13) we consider a torus $T^2 = S^1 \times S^1$ that consists of the points (k, ζ) [or, to be more precise of $(e^{ik}, e^{i\zeta})$], and note that a solutions of Eq. (4.13) can be represented as an intersection point on the torus T^2 of the closed curve C defined by the equation

$$\zeta = 2kL + \phi_A(k) + \phi_B(k) \tag{4.14}$$

with a simple circular curve C_0 defined by $\zeta = 0$ (an illustration is given in Fig. 4.7 in Section 4.3.2). We also note that, because the scattering phases satisfy the conditions $\phi(0) = \pi$ and $\phi(\pi) = 0$, there are two solutions (intersections) with $k = 0$ and $k = \pi$, respectively, which do not correspond to physical excited states, being represented by zero wave functions.

The reason for relating the number of excited states to the number of intersection points of two curves on a torus is to apply the concept of *intersection index* [86], denoted by $C * C_0$.

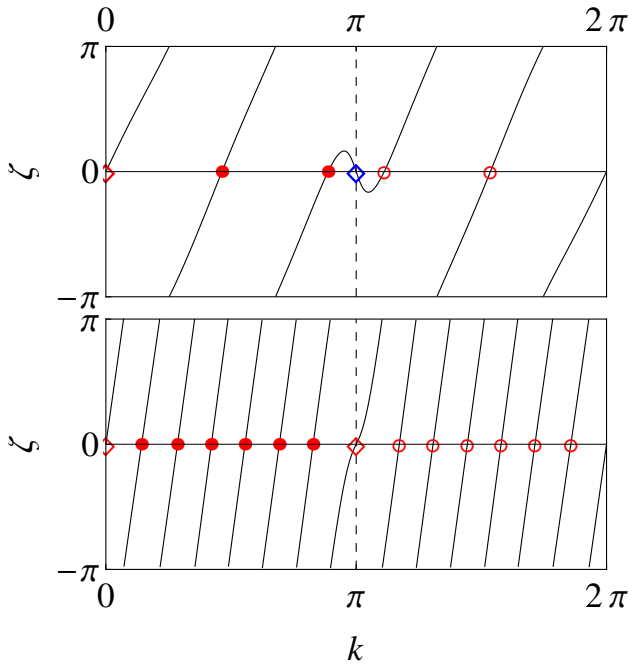

Figure 4.7: Graphical solution of Eq. (4.13) is represented as finding intersections of two closed curves on the torus. The fundamental polygons of the torus are shown for the A^0B^0 states in symmetric X molecules with arm lengths of two (top) and seven (bottom) repeat units. Circles and diamonds denote formal solutions (intersections): physical solutions in the first Brillouin half-zone (filled circles), their counterparts in the second half-zone (open circles), and unphysical solutions $k = 0$ and $k = \pi$ (diamonds). The symbols are red and blue for positive and negative individual intersection indices, respectively. The number of states in the band is represented by the number of filled circles.

If the curves intersect transversally (i.e., their tangent vectors at any intersection point are linearly independent), the intersection index is given by

$$C * C_0 = \sum_{\boldsymbol{x} \in C \cap C_0} \mathrm{ind}_{\boldsymbol{x}}, \tag{4.15}$$

where the intersection index $\mathrm{ind}_{\boldsymbol{x}} = \pm 1$ of an individual intersection point is determined by the relative orientation of the tangent vectors of the curves at the considered intersection point and in our case is given by

$$\mathrm{ind}_{(k,\zeta)} = \mathrm{sign}\left(d\zeta(k)/dk\right), \tag{4.16}$$

where $\zeta(k)$ is given by Eq. (4.14).

The intersection index can be used to count the number of intersections of two curves by utilizing its property of being a topological invariant: $C * C_0$ is invariant with respect to continuous deformations of the curves, and is explicitly expressed in terms of the topological invariants of the latter [86]. More specifically, we have

$$C * C_0 = n_2(C)n_1(C_0) - n_2(C_0)n_1(C), \tag{4.17}$$

where for any curve C on the torus, $n_1(C)$ and $n_2(C)$ denote how many times the curve winds along the first and second cyclic coordinates on the torus, k and ζ, respectively. For our particular choice of the curves we have $n_1(C_0) = 1$, $n_2(C_0) = 0$, $n_1(C) = 1$, and $n_2(C) = 2L + m_A + m_B$. The first three equalities are obvious, and the last is obtained by calculating a winding number of $\zeta(k)$ similarly to Eq. (4.11). This results in

$$C * C_0 = \sum_{\boldsymbol{x} \in C \cap C_0} \mathrm{ind}_{\boldsymbol{x}} = 2L + m_A + m_B. \tag{4.18}$$

Recalling our earlier statement on the relation between the number of physical states N in the band to the total number of (unsigned) intersections between C and C_0, we have

$$N = 1/2 \sum_{\boldsymbol{x} \in C \cap C_0} |\mathrm{ind}_{\boldsymbol{x}}| - 1, \tag{4.19}$$

where, in particular one unphysical state (that corresponds to two unphysical intersections) is subtracted.

In a general situation the relation between the intersection index and the total number of intersection points is complex. When the curves are deformed, the intersections can appear and disappear, changing the total number of intersection points. However, the intersection index remains unchanged, since the transverse intersections appear and disappear in pairs with opposite individual intersection indices. Stated differently, the intersection index, being a topological invariant, is easy to compute, whereas we are actually interested in the total number of intersections.

The situation becomes simple when all individual intersection indices $\mathrm{ind}_{\boldsymbol{x}}$ have the same value. This happens for a sufficiently long linear segment, when $d\zeta(k)/dk > 0$ for all k, and

Eqs. (4.19) and (4.18) result in a general relation

$$N = L + Q_A + Q_B \tag{4.20}$$

that expresses the total number N of excitations in an exciton band in terms of the number L of repeat units between the termini and the topological charges Q_A and Q_B of the reflection phases, with a topological charge being explicitly expressed in terms of the scattering degree.

$$Q = \frac{1}{2}(m - 1) \tag{4.21}$$

Note that Eq. (4.20) should and does hold regardless of particular choices of the reference points x that affect the reflection amplitudes, according to Eq. (4.10). Indeed, a shift of the reference point x by 1 repeat unit changes the corresponding scattering degree m by 2, which results in the change of the topological charge Q by 1; the latter is compensated in Eq. (4.20) by the corresponding change of the number L of repeat units by -1. Stated differently, the definition of the scattering phase is consistent with the corresponding agreement on the number of repeat units. Typically, with our definition of the reference point for the reflection phase, the scattering degrees m are odd numbers, so that the corresponding topological charges Q that enter Eq. (4.20) are integers.

For most scattering phases that we found in PA oligomers, $Q = 0$, i.e., the phase increases by π when k changes from 0 to π, and the number of states in the exciton band is equal to the number of repeat units. This is the case also for the states of certain symmetry in the symmetric molecules with symmetric branching centers. In most cases we do not observe strong negative slopes of the phase as a function of wavenumber, which means that the number of states should equal the number of repeat units even in the shortest molecules. Indeed, this is exactly what we observe in quantum-chemical computations in these typical cases.

4.3.2 Topological analysis of the X-joints and *ortho*-joints

At the end of section 4.2 we have briefly discussed some interesting features observed in the energy (or, equivalently, wavenumber) dependence of the scattering phases characterizing the *ortho*-joint and X-joint (see Figs. 4.3, 4.5 and 4.6). In this subsection we apply the analysis of the number of exciton states inside the band, presented in subsection 4.3.1, to draw parallels between the characteristic features of the scattering phases and quantum-chemical results for equal-arm molecules with the *ortho*-joint or the X-joint. As noted in subsection 4.3.1, time-reversal symmetry implies $\phi(k) = -\phi(-k) = -\phi(2\pi - k)$, any scattering phase is completely described by its behavior on half of the Brillouin zone, where $0 \leq k \leq \pi$.

For phase ϕ_0 of an *ortho*-joint (see Fig. 4.3 and 4.6), which corresponds to the symmetric states, the $2\pi-$kink in the each half Brillouin zone makes its topological charge $Q = 1$. This feature indicates one additional state with the given symmetry inside the exciton band. The conclusion is confirmed by the results of quantum-chemical computation: the number of symmetric excitations in symmetric *ortho*-molecule with arm length L is equal to $L + 1$. The $2\pi-$kink of ϕ_0 indicates that the additional state is a resonance around a certain energy for any arm length. The width of such resonance is positively related to the strength of the coupling between the state of the *othor*-joint and the excitations in the linear segments.

Although we do not have enough data for the phases of the X-joint at the band edges, the overall behavior of the phases ϕ_{10} and ϕ_{01} indicates that they change by 3π and $-\pi$, respectively, over the half of the Brillouin zone. The evidence in the case of the A^0B^0 symmetry is not as clear as for the first two cases. Nevertheless, the behavior of ϕ_{00} suggests that it has $Q = -1$ and a fast decrease near $k = \pi$ (we can expect ϕ_{00} to be equal to 0 at $k = \pi$ due to the observed slope and curvature, although we do not have sufficient data to confirm this property). Finally, the phase ϕ_{11} seems to change by π over the half Brillouin zone, i.e., by the same amount as all of the phases of the other PA vertices studied (see Figs. 4.4 and 4.3 as well as Ref. [80]), including the reflection phase at the unmodified PA terminus (phenyl ring).

Thus, we find three distinct cases for the scattering phases of the X-joint: $Q = 0$ for ϕ_{11}, $Q = 1$ for ϕ_{10}, and $Q = -1$ for ϕ_{01} and ϕ_{00}. The following detailed analysis in the equal-arm X molecules with free ends will also use that the unmodified PA terminus is characterized by $Q = 0$.

For the phase ϕ_{10} with a 2π-kink in each half of the Brillouin zone, we have $Q = 1$, which, according to Eq. (4.20), should result in one additional state inside the band. Indeed, the number of A^1B^0 states in quantum-chemical computations in X molecules with the arm length L is equal to $L+1$. Moreover, the abrupt change of ϕ_{10} implies that the additional state is a resonance at almost the same energy for any arm length, as observed. Correspondingly, in quantum-chemical transition density matrices, such states look like superpositions of a state localized on the X-joint and standing waves with reduced amplitudes in the arms. The width of the kink in ϕ_{10} can be interpreted as the strength of the coupling between the state on the X-joint and the excitations in the linear segments; the small width points to weak coupling. In other words, the kink in the scattering phase is a signature of the peak in the density of states that would be found in the X molecule with semi-infinite arms.

The phase ϕ_{01} is characterized by a relatively uniform negative slope and topological charge $Q = -1$, which, according to the analysis in the previous subsection, implies that for all arm lengths there is one fewer state of the symmetry A^0B^1 in the exciton band. Indeed, although in quantum chemistry results for X molecules with the identical arm length L there are L states with the A^0B^1 symmetry, one of them is always bound with its energy below the band. Thus, we see that such a gradual decrease of the scattering phase with $Q = -1$ is associated with the conversion of one of the states of the band into a strongly bound state.

For a long enough arm length L, one should have $L - 1$ excitations with the A^0B^0 symmetry inside the band. In the molecules with an arm length $L \leq 5$, quantum chemistry provides L excitations with the A^0B^0 symmetry, and we do not have high-energy results for bigger molecules due to computational limitations. Nevertheless, based on the data obtained from the molecules where quantum-chemical computations are still possible, the resulting

trend in the phase ϕ_{00} corresponds to an observation that the last excitation approaches the band edge relatively fast as the arm length increases. In addition, according to our preliminary results on analytic continuation of the scattering amplitudes to complex values of k, the curvature in the dependence $\phi_{00}(k)$ may correspond to the bound state above the band, in contrast to the shape of $\phi_{01}(k)$, for which the bound state is below the band. Thus, our observations for the A^0B^0 symmetry, although incomplete, do not contradict the general analysis presented in the previous subsection. We expect that in the X molecules with longer arms one will find a weakly bound state above the band converted from the state in the band. Alternatively, one can say that a state weakly bound at an end of a long segment enters the band when the segment becomes so short that the scattering at its other end sufficiently changes the state energy. In Fig. 4.7 we illustrate an application of the analysis of subsection 4.3.1 to A^0B^0 states in symmetric X molecules: we first interpolate $\phi_{00}(k)$ and the reflection phase $\phi_T(k)$ of the terminus in the whole Brillouin zone and then show the closed curve $\{(k,\zeta)|\ \zeta=\zeta(k)\}$ [see Eq. (4.14)] in the fundamental polygon (in this case, a square) $\{(k,\zeta)|\ k\in[0,2\pi),\zeta\in[-\pi,\pi)\}$ of the torus. Solutions of $\zeta(k)=2\pi q$ [Eq. (4.13)] are shown as intersections on the torus for two molecules with different arm lengths. The degrees of the scattering phases involved (ϕ_T and ϕ_{00}) are $m_T=1$ and $m_{00}=-1$, respectively. Therefore, according to Eq. (4.18), the total intersection index should be $C*C_0=2L$ for the symmetric X molecules with the arms of length L. In the molecule with $L=2$, the upper panel of Fig. 4.7 shows two A^0B^0 states in the band (since the solution $k=\pi$ has a negative intersection index, the total number of solutions in the Brillouin zone is $C*C_0+2=6$, of which 2 are unphysical, which yields $(6-2)/2=2$ states in the band). In the molecule with $L=7$, the lower panel of Fig. 4.7 shows six A^0B^0 states in the band ($L=7$ is big enough for all solutions to have positive intersection indices, and the total number of solutions in the Brillouin zone is $C*C_0=14$, of which 2 are unphysical, which yields $(14-2)/2=6$ states in the band).

In conclusion, in relatively small symmetric molecules with the X-joint we observe one

bound A^0B^1 state from the exciton band and introduces an additional A^1B^0 state inside the band. In fact, for energies below and above the kink in ϕ_{10}, the excitations of different symmetries appear in the order determined by the decreasing phase values at a given energy (A^1B^0, A^1B^1, A^0B^0, A^0B^1, A^1B^0, ..., see Fig. 4.5), while the inserted A^0B^1 state violates the order in the region of the kink. Thus, the available data on the number of states and their symmetries, obtained via quantum chemistry computations for symmetric X molecules, are in complete agreement with the analysis presented in the previous subsection. Similar comparison for other vertices, which all have $Q = 0$, also confirms the relation (4.20); those simpler situations are not discussed here.

4.3.3 Topological properties of the scattering matrices and the lattice-model description

Thus far, we have presented an initial analysis of the relations between the number of the exciton states in the band, the number of repeat units, and characteristic features of the scattering phases, as functions of the wavenumber. We observed that the phases of the X-joint corresponding to different symmetries exhibit different types of behavior and found that their features are in agreement with the quantum-mechanical results for symmetric X molecules. These results provide another demonstration of the usefulness of the ES approach for understanding electronic excitations in conjugated molecules.

We conclude with indicating several directions of our future research with the ultimate goal of developing an efficient computational approach for description and analysis of electronic and optical properties of large branched conjugated molecules. We are following the way common in condensed matter physics: first we identify and characterize free noninteracting particle-like excitations (excitons), and later intend to characterize their interactions with phonons and static disorder. This will allow us to build efficient approaches for treating not only light absorption but also photoinduced dynamics, including energy transfer, in realistic imperfect oligomers.

As a way to actualize this program we have to reduce the number of parameters used for description of electronic excitation and study their dependence on geometrical distortions. We already observed [39, 43] that the exciton dispersion $\omega(k)$, extracted from the quantum-chemical computations, can be adequately approximated by a small number of cosine harmonics, which is exactly the form one finds in tight-binding lattice models with possible hopping between close neighbors. We have reasons to believe that the frequency/wavenumber dependence of the scattering matrices can also be represented by a few lattice model parameters. Thus, instead of high-dimensional parametrization of the full ES approach (which involves fitting functions on several intervals), we will deal with a reasonably small number of meaningful parameters, associated with the effective exciton lattice model, that will be obtained from the reference quantum-chemical method via the ES methodology. In addition, analytical expressions for the scattering matrices derived within a lattice model can be used for analytic continuation, which will allow us, in particular, to deduce the positions of possible bound states from the scattering phases. Thus, the analysis of analytical and topological properties of the scattering matrices initiated in this work will be completed with the help of the lattice-model description to eventually serve as an important criterion for choosing an appropriate lattice model.

Chapter 5

Effective tight-binding models for electronic excitations in conjugated molecules

In this chapter, we introduce an efficient description of electronic excitations in terms of effective tight-binding (lattice) models whose parameters and morphology are determined from the ES parameters (exciton dispersion relation and energy-dependent scattering matrices). The topological and analytical properties of the scattering matrices investigated in Chapter 4 guarantee adequate representation of the corresponding molecular vertices within the tight-binding models. Since the electronic excitations can be characterized by only a small number of constants depending on the molecular geometry only, the approach of tight-binding models can be used to investigate photoinduced dynamics in conjugated molecular systems and constitutes a new level of the ES theory.

5.1 Effective tight-binding model representation of the exciton states

According to previous investigation on exciton scattering in organic conjugated molecules, we know that strong electron correlations result in the small size of exciton, which is about 1-3 repeat units in phenylacetylene (PA) based molecules. This fact is also confirmed by the expansion of the exciton dispersion relation $\omega(k)$ using Fourier series in terms of quasi-

momentum k (see Fig. 5.1). The ES picture holds for low-dimensional geometries and excitons with tight binding energies. These knowledge implies that we can introduce effective tight-binding models for the particular exciton type in which molecular vertices with localized exciton effect could be described by the geometry-dependent tight-binding constants (i.e., the on-site energies Ω and hopping constants J) instead of those energy-dependent ES parameters.

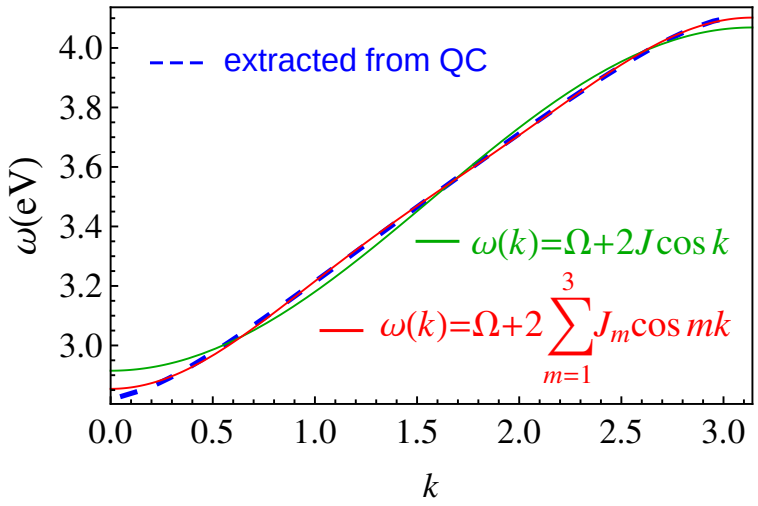

Figure 5.1: The extracted exciton dispersion from TDHF (CEO) energies fitted with one and three cosines.

More specifically, a tight-binding model is defined on a graph (i.e., an irregular lattice) as shown in Fig. 5.2. Repeat units that form the linear segments of the considered branched molecule are represented by single sites, whereas the molecular vertices (i.e., termini with and without substituent, *meta*-joint and symmetric quadruple joint) are generally represented by combinations (subgraph) of linked sites.

In the simplest class of lattice models where each repeat unit corresponds to a lattice site, the system without external optical field is described by the exciton Hamiltonian [87, 88]

$$H \equiv \sum_{m} \omega_m B_m^{\dagger} B_m + \sum_{m,n}^{n \neq m} J_{mn} B_m^{\dagger} B_n, \tag{5.1}$$

where $B_m^{\dagger}$ and B_m are creation and annihilation operators of an exciton on lattice site m,

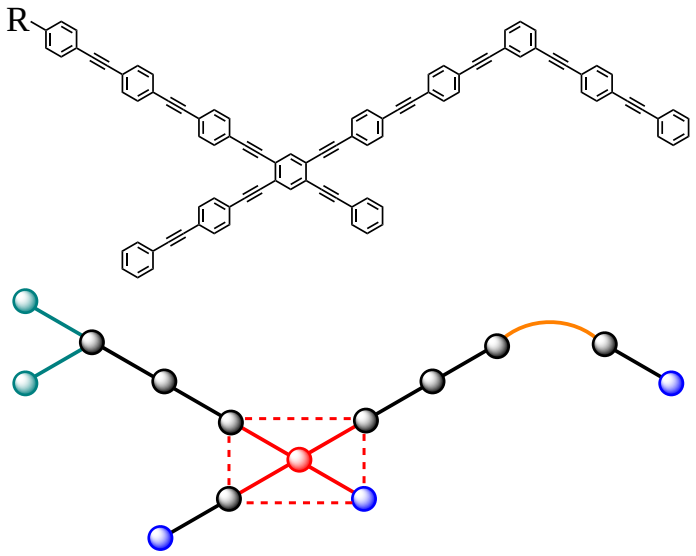

Figure 5.2: An example of a conjugated molecule and a graph for a possible tight-binding model. Different colors of sites and links represent different on-site energies and hopping constants.

respectively. ω_m represents the corresponding on-site energy. J_{mn} is the lattice hopping constant, i.e. the exciton transfer matrix element between the two sites m and n.

The eigenstates can be found through the exciton Hamiltonian. The exciton wave function of eigenstate j is specified by the jth eigenvector with amplitude A_{jn} on lattice site n

$$|\Psi_j\rangle = \sum_n A_{jn}|n\rangle\,. \tag{5.2}$$

In an infinite linear chain, the on-site energy is a constant ω_0 due to the discrete translational symmetry. The hopping constants depend only on the distance between the two sites: $J_{mn} = J_{nm}$. Then, the analogue of the Schrödinger equation of exciton is simplified as

$$\sum_m J_m(A_{n-m} + A_{n+m}) = (E - \omega_0)A_n, \tag{5.3}$$

where the subscript m denotes the hopping distance and n is the index of lattice sites. In an infinite chain Eq.(5.3) has a plane-wave solution $\propto e^{ikx}$ with the energy

$$E(k) = \omega_0 + 2\sum_m J_m \cos mk, \tag{5.4}$$

where k denotes the wavenumber. This equation describes the exciton dispersion relation in the form of Fourier series and indicates the width of the exciton band is $2\sum_m |J_m|$ and the center of the exciton band is ω_0. Consequently the number of the significant cosine harmonics in the Fourier series expansion tells us the allowed hopping distance m. If there are other nonzero hopping constants beyond J_1, equation (5.3) has wave solutions with complex wavenumbers.

In a real molecule, molecular vertices violate the discrete translational symmetry of the polymer chain and thus cause exciton scattering, which makes quasimomentum k quantized. The solution of Eq. (5.3) is generally different from the standing wave. This effect can be modeled by the variation of the on-site energies and hopping constants near the vertices, or introducing additional lattice sites represent the vertex. By comparing the profile of the exciton wave function extracted from the result of quantum chemical computation to the standing wave form from the ES approach, one can tell that the effect of a scattering center is typically localized within several repeat units [65], the molecular vertex only affects a finite number of lattice sites. To find elements of the scattering matrix of a vertex within the lattice model, one assumes that there is only one incoming wave that has a form $\propto e^{-ikx}$ far from the vertex and, by solving the set of wave equations (5.3), finds outgoing waves in all linear branches attached to the vertex. Consequently the scattering amplitudes are analytically obtained.

Furthermore, because the eigenstate is found from the wave equation (5.3) set, the dimension of the eigenvector, i.e. the number of excitations, is determined by the number of lattice sites. This argument helps us build decent lattice model for different molecular systems. In Chapter 4 the relations between the number of the exciton states in the band, the number of repeat units and the topological properties of the scattering phases are described by Eq. (4.20), which indicates that the molecular vertices alter the number of excitations in addition to the length of the molecule. In addition, the number of the states is equal to the number of the lattice sites within a lattice model. Therefore, in the lattice models for

phenylacetylene (PA) based molecules with respect to the previously studied exciton type, each repeat unit in linear segment should be represented by one single lattice site, whereas the number of the lattice sites describe a molecular vertex should be determined by the topological and analytical properties of the corresponding scattering phases [Eq. (4.21)]. As a result of the topological analysis on scattering phases, the structure of the lattice model could be uniquely determined for a given molecule with all building blocks characterized.

Since any scattering with certain symmetry can be studied as an reflection using effective linear segment model (see 4.2.1 and 4.2.2), we can start with the lattice models describe linear chains. In these models regardless of the allowed hopping distance, the reflection amplitude has a universal form

$$r(k) = -e^{ik}\frac{P(e^{-ik})}{P(e^{ik})}, \tag{5.5}$$

where $P(z)$ ($z = e^{ik}$) is a polynomial with real coefficients, i.e. $[P(z)]^* = P(z^*)$. Zeros of $P(z)$ at $|z| > 1$ correspond to bound states. At $k = 0$ the reflection phase $\phi_T = \pi$. When k increases from 0 to π, the reflection phase increases to 2π if there are no bound states or decreases by $\pi + 2\pi(n-1)$ if there are n bound states. This argument agrees with the result of the topological analysis of the scattering phases in 4.3.1.

5.2 The simplest tight-binding model based on the ES approach

In this section we illustrate the application of tight-binding models using the simplest model describes a linear molecule. Molecular terminus and nearby repeat units of the lattice model is shown in Fig. 5.3. Here only the nearest neighbor hopping J_1 is considered and each lattice site represents one repeat unit. The simplified exciton dispersion relation $\omega(k) = \omega_0 + 2J_1 \cos k$ indicates the exciton band is in between $\omega_0 \pm 2J_1$. The exciton wave function is a standing wave

$$\psi(x) = r_0(k)e^{ikx} + e^{-ikx}, \tag{5.6}$$

where $r_0(k)$ is the reflection amplitude with respect to the reference point 0. The dependence of the reflection phase on a particular choice of the reference point is described by Eq. (4.10). Therefore the reflection amplitude $r(k)$ within the ES approach defined at 1/2 can be found from $r(k) = r_0(k)\exp(ik)$.

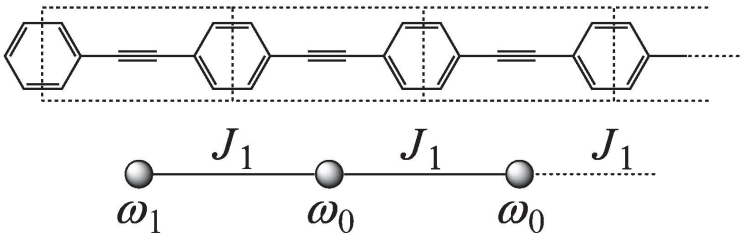

Figure 5.3: The simplest lattice model for linear molecule.

In the simplest lattice model, since there is no lattice site represent the molecular terminus, the terminal effect is parameterized by the variation of the on-site energy ω_1 of the site next to the terminus, i.e., the on-site energy of the furthest site from the molecular center. Then, from the lattice equation 5.4 at the first site, the reflection amplitude can be found as

$$r(k) = -e^{ik}\frac{ge^{-ik}+1}{ge^{ik}+1}, \tag{5.7}$$

where $g = -(\omega_1 - \omega_0)/J_1$. The bound state localized in the vicinity of the terminus indicates zero reflection amplitude, the complex wavenumber, and $|e^{-ik}| < 1$. The bound state exists if $|g| > 1$, i.e., if the difference between energies exceeds the value of the hopping constant, i.e. a quarter of the band width. For negative and positive g, the bound state can be either below or above the exciton band, respectively. In other words, the tight-binding representation of the reflection amplitude allows for analytic continuation of $r(k)$ to complex values of k, which correspond to the bound exciton states whose energies are outside of the exciton band. Figure 5.4 shows possible shapes of the reflection phase when the terminus is characterized by one varied on-site energy. The relation between the topological charge Q of the phase and the parameter g has been clearly described.

This example demonstrates that even the simplest lattice model can describe the exciton

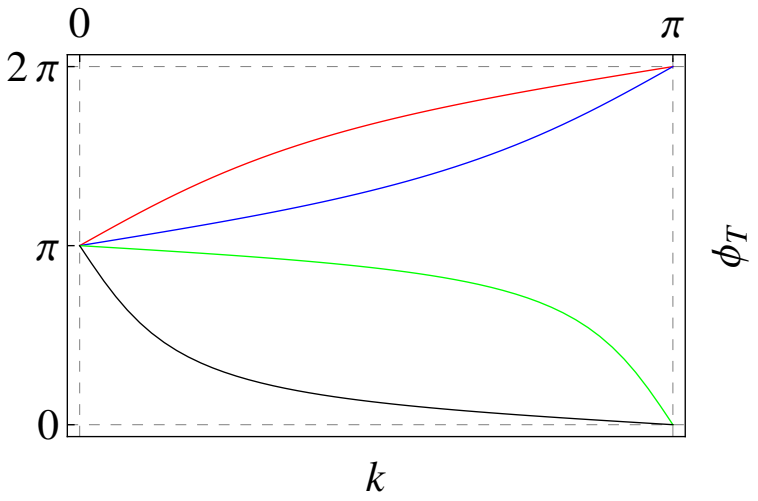

Figure 5.4: Possible shapes of the reflection phase at the terminus characterized by one on-site energy with the nearest neighbor hopping in the chain, for four values of g: -0.3 (red), 0.3 (blue), 1.5 (green), and -1.5 (black). The topological charge $Q = 0$ when $|g| < 1$, $Q = -1$ when $|g| > 1$.

scattering at molecular vertices qualitatively. The exciton dispersion $\omega(k)$ is parameterized by two constants, the on-site energy ω_0 and the nearest neighbor hopping constant J_1. The energy-dependent reflection phase ϕ_T in the ES approach is replaced by the lattice constant ω_1. In such way, the description of the excited states in conjugated molecules has been greatly simplified. The study on geometry-dependent electronic excitations becomes possible.

5.3 The tight-binding models for the localized excitons

Like the exciton scattering analysis, the representation of tight-binding models can be applied to any exciton band. By inspecting the transition density matrices obtained from the quantum-chemical computation using CEO code [46, 47, 63, 64], we observed two exciton bands at low energy [43]. The lowest exciton band with band width about 1 eV is referred to as delocalized exciton or light exciton band, whereas the narrower exciton band (width of 0.1 eV) embedded in the delocalized band is referred to as localized or heavy exciton band [43]. The dispersion relation of localized exciton is accurately described by the second order

Fourier series expansion

$$\omega(k) = \omega_0 + 2J_1 \cos k + 2J_2 \cos 2k, \tag{5.8}$$

with $\omega_0 = 3.35852$ eV, $J_1 = -0.0228314$ eV, and $J_2 = 0.0000542$ eV. The lattice constants are found by fitting the exciton dispersion using Eq. (5.8). Because $|J_1| \gg |J_2|$, lattice models of the nearest neighbor hopping are accurate enough to describe the exciton dispersion, which is shown in Fig. 5.5.

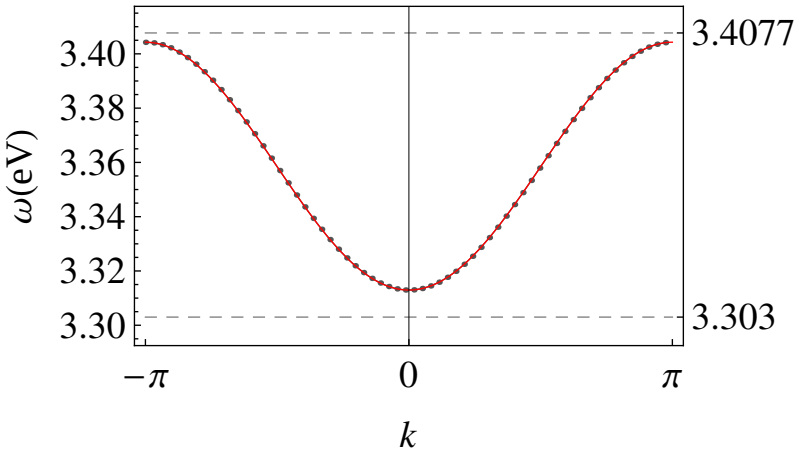

Figure 5.5: The dispersion (gray dots) of localized exciton fitted with one cosine (red curve). The bound state energies of the NO_2 and NH_2 substituted molecules are 3.3030 eV and 3.4077 eV, respectively.

We study the localized exciton using tight-binding models for two reasons: the exciton dispersion is precisely described by a single cosine, and the bound states have been observed in the quantum-chemical results of two donor/acceptor substituted molecules (see Fig. 5.5). Same as Chapter 3, we consider linear PA molecules with molecular termini substituted by -NH_2, -CF_3 and -NO_2 in *para* position (see inset of Fig. 3.1). The dispersion relation $\omega(k)$ and the reflection phase ϕ_T of the unmodified terminus have been extracted from the quantum chemical results of several linear molecules, like we did for the delocalized excitons [43]. Then the phases of the modified termini can be calculate from Eq. (3.1). All the reflection phases of localized exciton at the four studied termini are shown in Fig. 5.6.

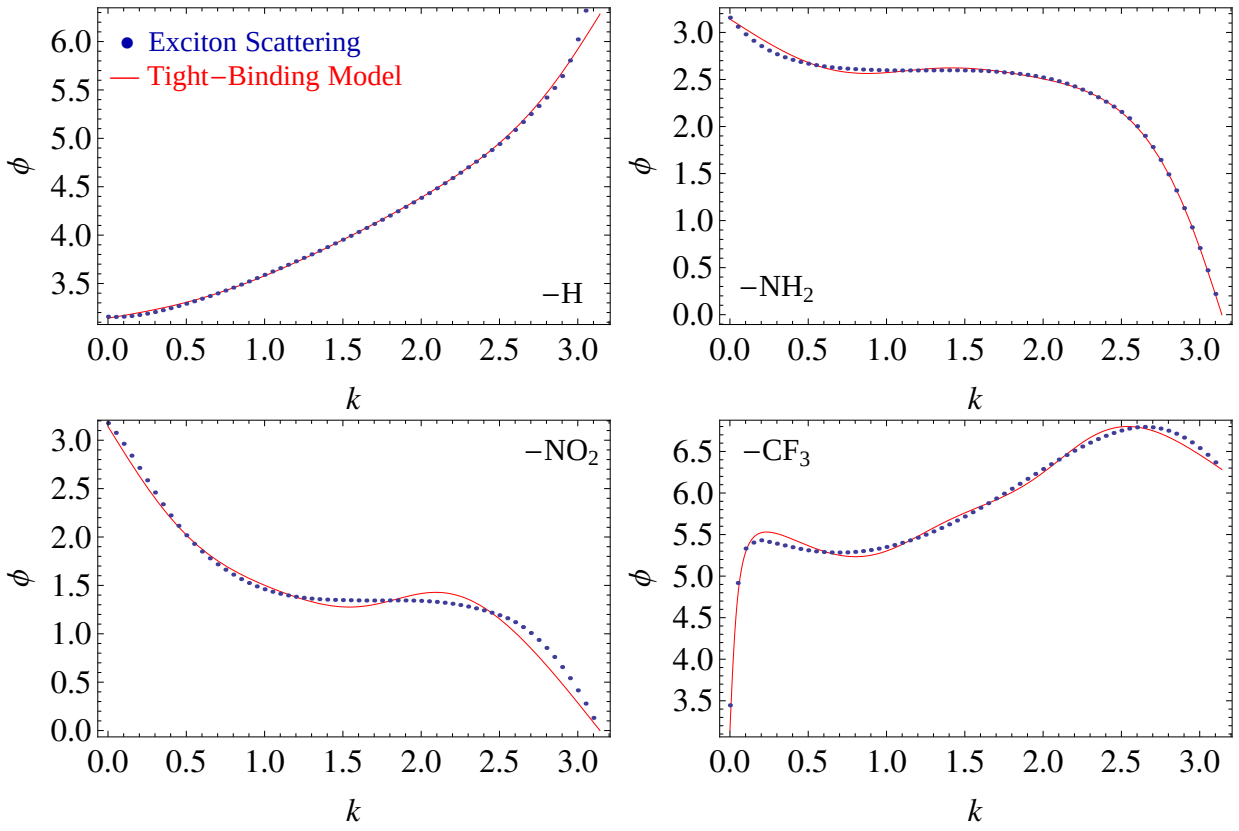

Figure 5.6: Reflection phases of localized exciton at the four terminals: (from top to bottom) regular benzene ring, NO_2, NH_2, and CF_3. Blue dots are from exciton scattering analysis on quantum chemical results, and red curves are the best fits using the lattice model. There are bound states for NH_2 and NO_2 substituted molecules.

For the phases ϕ_T of unmodified terminus and ϕ_{CF_3} of -CF_3 substituted terminus, the topological charge $Q = 0$. This indicates the termini would not affect the number of the excitations. The phases ϕ_{NO_2} and ϕ_{NH_2} are characterized by negative slope and the topological charge $Q = -1$. According to the qualitative results of the simplest lattice model in Section 5.2, one can predict the presence of the bound state and tell its position relative to the exciton band. In all the four types of studied molecules, the number of the localized excited states, including bound state outside the band, are identical with the length of the molecule L. Therefore, in the lattice models for such molecules with respect to localized exciton, each lattice site represents one repeat unit. The number of the lattice parameters describing the molecular vertex depends on the features of the corresponding phase. For ex-

ample, the unmodified terminus can be characterized by only one varied on-site energy since the profile of the phase is simple. However, at least two varied on-site energies are necessary for electron donor and acceptor substituted termini because the corresponding phases are more complicated.

The nearest neighbor hopping lattice model (characterized by on-site energy ω_0 and hopping constant J_1) has been used n Fig. 5.6. The terminal effect is parameterized by three varied on-site energies (ω_1, ω_2 and ω_3), which correspond to the three lattice sites near the terminus, and one varied hopping constant (K_1) between the two sites near the terminus. These four lattice parameters have been obtained from the best fits of the reflection phases. Following this idea, the exciton behavior at a molecular vertex is characterized by a small number of lattice constants. Analytic continuation of the reflection amplitude in the lattice model allows one to identify the bound states in molecules with substituents of NH_2 and NO_2. The obtained lattice constants lead to the bound state energies 3.4083 eV and 3.2946 eV in NH_2 and NO_2, respectively, which are close to the reference quantum chemical results, 3.4077 eV and 3.3030 eV.

5.4 The tight-binding models for the delocalized excitons

5.4.1 The lattice models describe electron donor and acceptor substituted molecules

In this section we investigate the lowest exciton band (delocalized exciton) using tight-binding models. The dispersion relation of delocalized excitons requires at least three cosine harmonics to be accurately characterized. This indicates the allowed couplings are the nearest neighbor, next nearest neighbor and the third neighbor hopping, which are parameterized by coupling strength J_1, J_2 and J_3 respectively. The exciton dispersion is described by the expression

$$\omega(k) = \omega_0 + 2J_1 \cos k + 2J_2 \cos 2k + 2J_3 \cos 3k, \tag{5.9}$$

where $\omega_0 = 3.49052$ eV, $J_1 = -0.29303$ eV, $J_2 = -0.00618$ eV, and $J_3 = -0.01847$ eV. These values are obtained by fitting the dispersion from quantum-chemical results, as shown in Fig. 5.1. For a given energy Eq. (5.9) has three solutions of k. Two of the solutions correspond to the complex wavenumbers κ_a and κ_b. Therefore the wave function of such lattice model has a general form

$$\psi(x) = r_0(k)e^{ikx} + e^{-ikx} + b_1(k)e^{-i\kappa_a x} + b_2(k)e^{i\kappa_b x}, \tag{5.10}$$

where the reflection amplitude $r_0(k)$, coefficients $b_1(k)$ and $b_2(k)$ can be found by solving the lattice equantion (5.3) set.

First we apply such third-neighbor-hopping tight-binding model to the linear molecules with NH_2, NO_2 and CF_3 substituted termini (see inset of Fig. 3.1). Three on-site energies and one nearest neighbor hopping constant in the vicinity of the terminus have been varied for the terminal effect. The results of such lattice model are shown in Fig. 5.7.

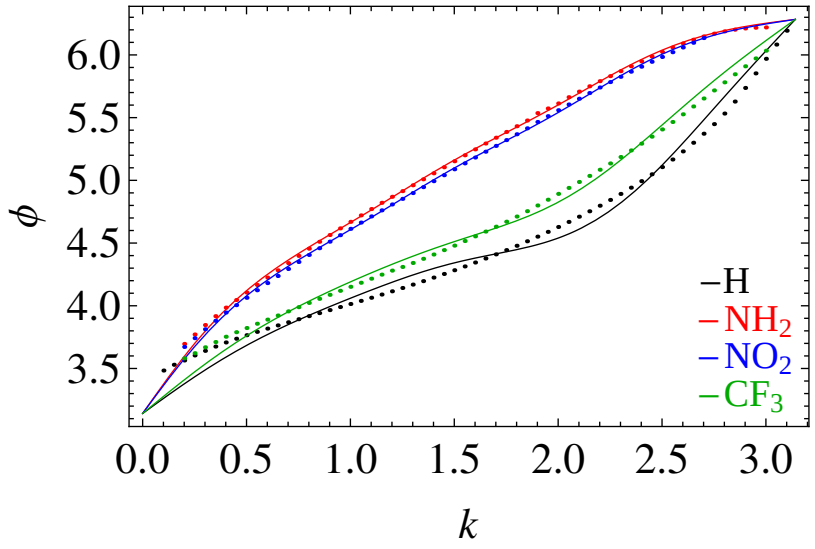

Figure 5.7: Reflection phases of delocalized exciton at the four terminals: (from bottom to top) regular benzene ring, CF_3, NO_2, and NH_2. Dots are from exciton scattering analysis on quantum chemical results, and the curves are the best fits using the third-neighbor-hopping lattice model.

Although considering the third neighbor hopping for delocalized exciton better approximates the dispersion relation, longer hopping range makes the tight-binding models difficult

to process analytically. The wave function yields to a complex form Eq. (5.10), the description of the molecular vertex requires more lattice parameters as well. Consider that the nearest neighbor hopping constant J_1 is still greater than long range hopping constants J_2 and J_3, we test the nearest-neighbor-hopping lattice models in delocalized exciton band. The relevant lattice parameters $J_1 = -0.28783$ eV and $\omega_0 = 3.49207$ eV are from the fit of the dispersion using single cosine. Less number of parameters have been used for the four studied termini: two varied nearby on-site energies and one varied hopping constant between the first two sites. The sketch of the lattice model is shown in Fig. 5.8 while the results of the lattice model is shown in Fig. 5.9. Such simple models also reproduce the ES phases very well. From the lattice model we conclude there is no bound state of delocalized excitons, which agrees with the quantum-chemical results.

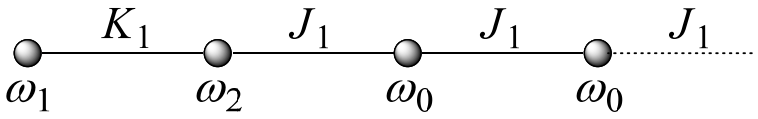

Figure 5.8: The nearest-neighbor-hopping lattice model for linear molecules. Exciton behavior at the terminus is parameterized by K_1, ω_1 and ω_2.

Comparing Fig. 5.7 to Fig. 5.9, we observe that allowing longer hopping distance cannot improve the description of exciton scattering, even it is necessary for accurate approximation of the dispersion. The number of the tight-binding parameters describe molecular vertices are more important especially for the vertex with complex phases. Therefore, we always apply the nearest-neighbor-hopping models, as the first trial, to a new molecular system. To improve the accuracy of lattice model, increasing the number of lattice parameters describe the vertex takes priority over introducing longer hopping range. In the rest part of this chapter, only the nearest neighbor hopping is considered.

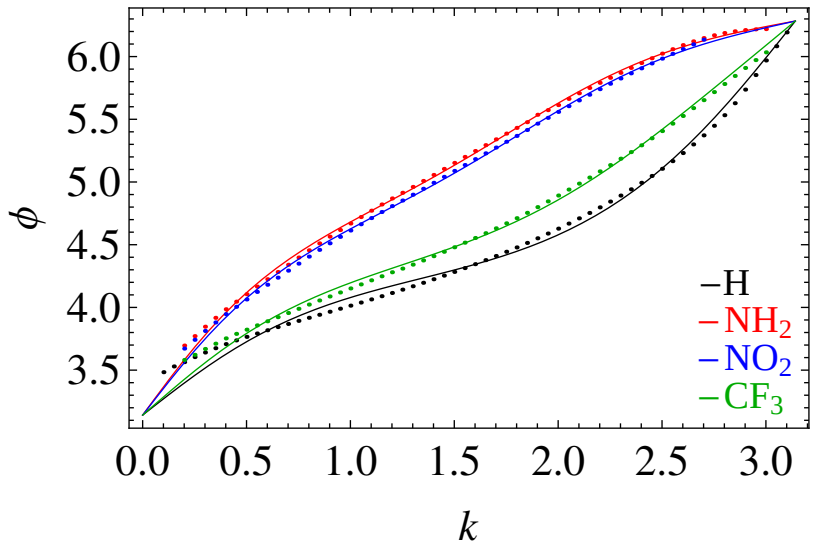

Figure 5.9: Reflection phases of delocalized exciton at the four terminals: (from bottom to top) regular benzene ring, CF_3, NO_2, and NH_2. Dots are from exciton scattering analysis on quantum chemical results, and the curves are the best fits using the nearest-neighbor-hopping lattice model.

5.4.2 The lattice models for molecules contain symmetric V-, Y- and X-joints

At a symmetric molecular vertex, the scattering with certain symmetry can be treated as an effective reflection in a linear chain [89]. Based on this argument, the lattice constants characterize such symmetric joints can be determined easily. Since there are more than one phase for symmetric double (V-), triple (Y-) and quadruple (X-) joints, the corresponding lattice models may be complicated for the purpose of describing all scattering behaviors simultaneously.

The structure of a lattice model (including sites and links) can be determined from the molecular structure. Specifically, the number of the lattice sites is directly related to the topological charges Q of the corresponding scattering phases. The scattering phases of *meta* joint extracted from quantum chemistry results are shown in Fig. 5.10. The topological charges Q_0^M and Q_1^M of both phases is zero, which indicates the number of lattice sites N in such model is $L + 2Q_T + Q_0^M + Q_1^M = L$, where $Q_T = 0$ is the reflection phase of

the unmodified terminus and L is the length of the molecule. In the lattice model for a *meta*-conjugated molecule, as shown in Fig. 5.11, each lattice site represents one repeat unit. The *meta*-conjugation is parameterized by two varied on-site energies, one varied nearest neighbor hopping K_1, and three couplings J^M_{aa}, J^M_{ab} and J^M_{bb} around the joint.

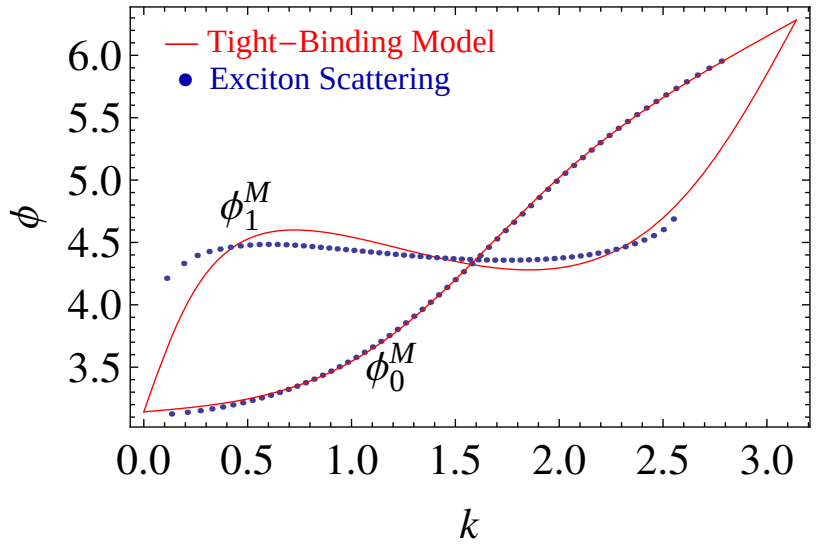

Figure 5.10: The scattering phases of the *meta(M)*-joint. Subscript 0/1 denotes symmetric/antisymmetric scattering.

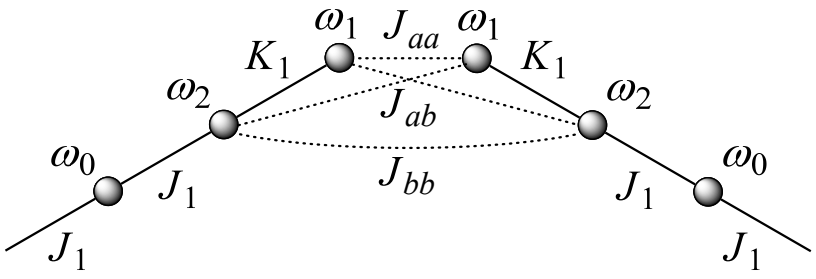

Figure 5.11: The lattice model describe the *meta(M)*-joint. Dashed line represents weak coupling.

The coupling between the two repeat units connected by *meta* joint is measured by J^M_{aa}, which is found as -0.01594 eV from the best fits of the ES phases. Compared to the hopping constant in the chain $J_1 = -0.28783$ eV, weak coupling cross the *meta* joint is concluded. This result agrees with the impenetrable property of the *meta*-conjugation which has been

proved in quantum chemistry and organic chemistry. The two couplings J^M_{ab} and J^M_{bb} across the joint are necessary for the characterization of the scattering phases. Both couplings are found to be weak and comparable to J^M_{aa}. All of the three couplings across the joint are attributed to the weak Coulomb interactions. Using such lattice model the scattering phases of *meta* joint are characterized (see Fig. 5.10).

There is a resonance-type behavior in the scattering phase ϕ^O_0 of *othor* joint corresponds to symmetric scattering (see Fig. 5.12). The topological charge $Q^O_0 = 1$ indicates that the number of the exciton states in an *ortho*-conjugated molecule is $L + 1$ where L denotes the molecular length. Therefore, one additional lattice site should be used to represent the *ortho* joint in the lattice model for such molecule, shown in Fig. 5.13. In this model, the effect of *ortho*-conjugation is characterized by one extra lattice site (on-site energy ω_o and neighbor coupling J_o) in addition to two varied on-site energies several couplings around the joint.

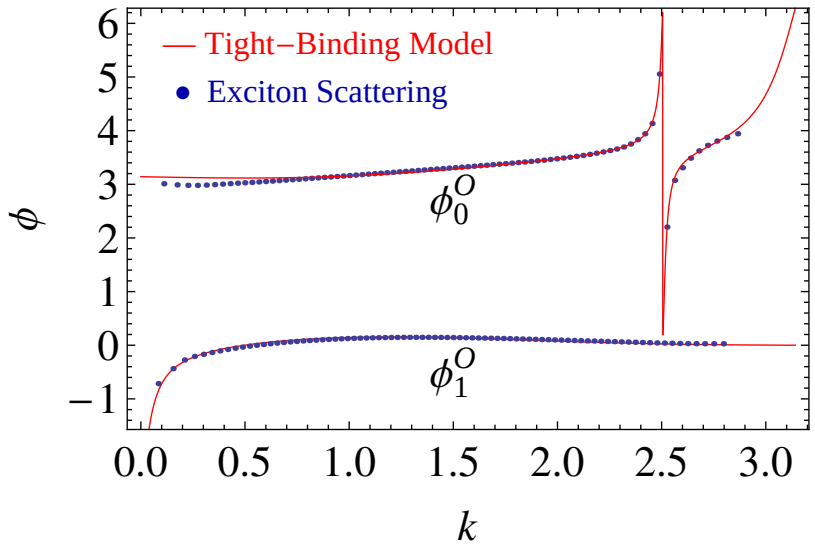

Figure 5.12: The scattering phases of the *ortho(O)*-joint. Subscript 0/1 denotes symmetric/antisymmetric scattering.

Not like in the *meta* joint, the coupling across the *ortho* joint between the two linked repeat unit $J^O_{aa} = -0.28036$ eV is as strong as the coupling in the linear chain. This result indicates that *ortho*-conjugation is almost as transparent as *para*-conjugation. We know the

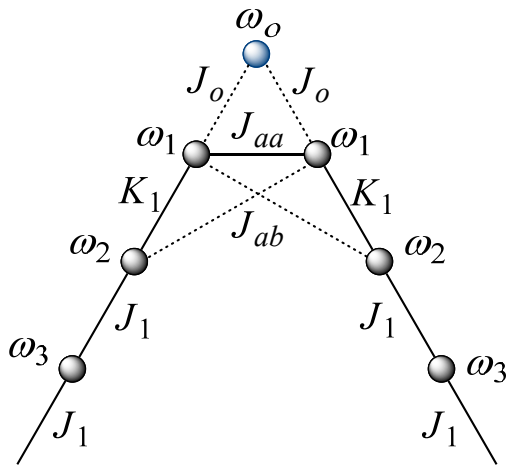

Figure 5.13: The lattice model describe the *ortho(O)*-joint. The joint is represented by the lattice site with on-site energy ω_o. Dashed line represents weak coupling.

abrupt resonance shape in phase ϕ_0^O corresponds to the extra resonant state at almost the same energy for any arm length [89]. This resonance can be interpreted as the coupling between the state at the joint and the excitations in the linear chains. The position of the resonant state is determined by the on-site energy $\omega_o = 3.95661$ eV. The width of the resonance is determined by the strength of the coupling $J_o = -0.02132$ eV. In other words, the sharp resonance feature of the phase within the ES approach is parameterized by the on-site energy ω_o the weak coupling constant J_o in the tight-binding models. Both scattering phases have been precisely described within the tight-binding models (see Fig. 5.12).

Following the same methodology, symmetric triple (Y-) and quadruple (X-) joints have been studied using the tight-binding models. No lattice site should be used for the Y- joint since the corresponding topological charges are zero. In the lattice model, all the lattice parameters are introduced or varied symmetrically. In each arm linked to the joint, the on-site energies of the two nearby lattice sites and the coupling strength between them are allowed to vary. The hopping whose distance is less than two repeat units is allowed between any two different arms. The hopping constants are referred to as J_{aa}^Y, J_{ab}^Y and J_{bb}^Y, ordered by the relevant hopping distance. The couplings between different arms are attributed to the weak Coulomb interactions. Since the coupling between repeat units connected by the Y-

joint actually characterizes the between the *meta*-positions of the phenyl ring, the strength of coupling $J^Y_{aa} = -0.01065$ eV determined from the lattice model is comparable to that across the *meta* joint $J^M_{aa} = -0.01594$ eV.

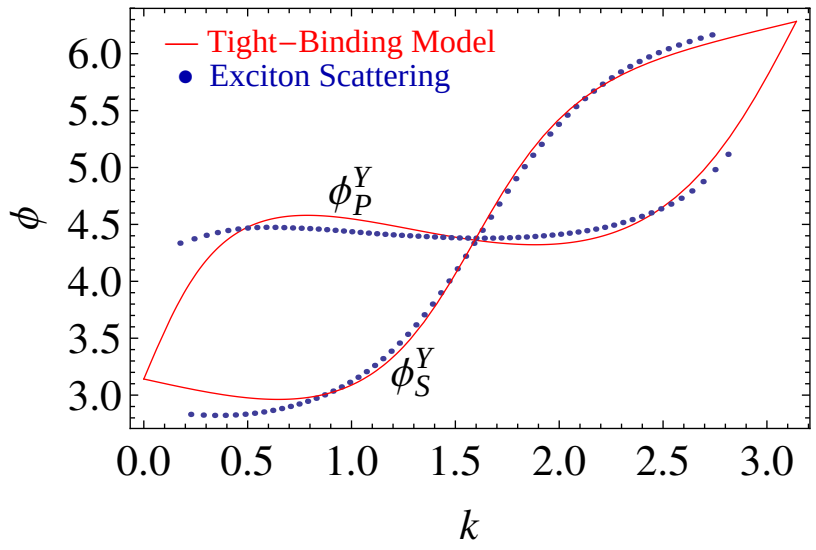

Figure 5.14: The scattering phases of the triple (Y-) joint. Subscript S denotes the states where the angular momentum $m = 0$, whereas P denotes the double degeneracy of the $m = \pm 1$ modes.

The exciton behavior at the X-joint is complicated because of the four distinct characteristic scattering phases (see Fig.5.15): topological charge $Q = 0$ for ϕ_{11}, $Q = -1$ for ϕ_{01} and ϕ_{00}, $Q = 1$ for ϕ_{10}. The correspond notations of symmetry can be found in Section 4.2. The scattering with the A^1B^0 symmetry results in one additional resonance state in the exciton band, where as the phases with symmetry A^0B^1 and A^0B^0 are responsible for the two bound states outside the band. Therefore, in the lattice model for a molecule with X-joint, the joint is represented by an extra site whose on-site energy is denoted by ω_x and the strength of coupling to linked sites is J_x. In order to describe the four phases simultaneously, the coupling across the X-joint is allowed only when the coupling distance is no longer than three repeat units. Two on-site energies and one hopping constant of the molecular arm in the vicinity of the joint are allowed to vary in the lattice model shown in Fig. 5.16.

The relevant lattice constants for the X-joint are obtained by fitting the scattering phases.

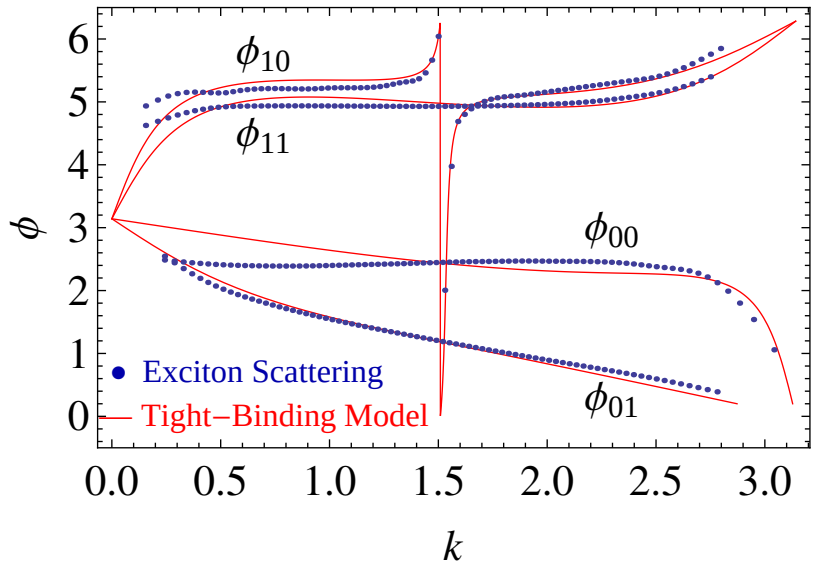

Figure 5.15: The scattering phases of the quadruple (X-) joint. Subscripts of the phase denotes the symmetry of scattering, which is defined in Section 4.2.

The sharp resonance shape of ϕ_{10} is attributed to the weak coupling between the X-joint and the linked repeat units whose strength $J_x = -0.02955$ eV is weaker than the coupling strength in the chain $J_1 = -0.28783$ eV. The energy of the site represents the joint $\omega_x = 3.46894$ eV matches to the energy of the resonant states. The strengths of couplings across the X-joint also agree with the results of *meta*- and *ortho*-conjugations, i.e., the hopping constant between the two sites linked on the *meta*-positions of the joint is comparable to the hopping constant $J^M_{aa} = -0.01594$ eV, whereas the strength of couplings over *ortho*- and *para*-positions are similar to the nearest neighbor hopping constant in the chain $J_1 = -0.28783$ eV.

Using the lattice-model description of the scattering with symmetry A^0B^1 and A^0B^0, the corresponding bound states have been predicted. Since the nearest neighbor hopping cannot accurately describe the exciton dispersion, in such lattice models, it is reasonable to compare with the quantum-chemical results using the distance between the bound state and the exciton band edge, other than comparing the absolute position of the bound state. The bound state with symmetry A^0B^1 predicted by the lattice model is 151 meV below the lower band edge and the CEO result is 78 meV below. The bound state with symmetry A^0B^0

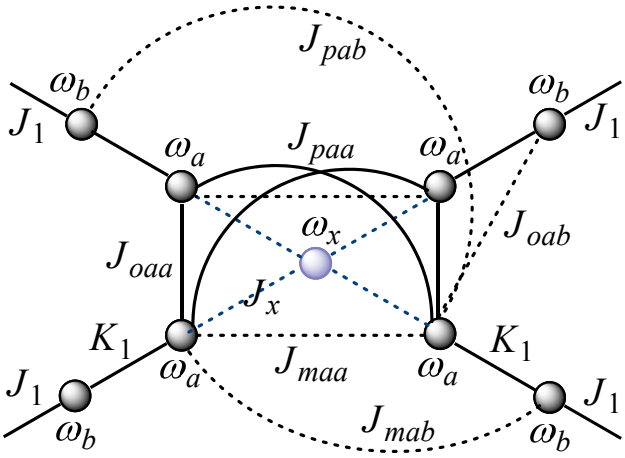

Figure 5.16: The lattice model describe the X-joint. The joint is represented by the lattice site in the middle with on-site energy ω_x. Dashed line represents weak coupling.

is predicted 5 meV above the exciton band whereas the bound state computed by CEO is missing because of the computational limitation. According to the topological analysis of the phase and the trend that the highest excitation approaches the upper band edge while the arm length increases, we expect that there will be a bound state above the exciton band in X-molecules with sufficiently long arms [89]. Therefore, such simple tight-binding representation is capable to provide immediate analytic continuations of the scattering matrix to complex values of k, which allows the prediction of the bound states, at least, qualitatively.

5.4.3 The lattice models for perylene substituted molecules

Perylene is a useful chemical structure which, as well as its derivatives, have applications as fluorescent materials and organic photoconductors. Attributed to the fluorescent feature, it is frequently used as energy traps in conjugated molecular systems such as the nanostar dendrimer [8, 9, 90]. In this section, perylene terminated linear phenylacetylene (PA) chain (see Fig. 5.17) have been studied as an example of perylene substituted molecules. Within the ES approach, the perylene termini can be characterized by the relevant ES parameters [80], including the scattering phase and transition dipole parameters. Based on the exciton scattering analysis, proper tight-binding model can be developed.

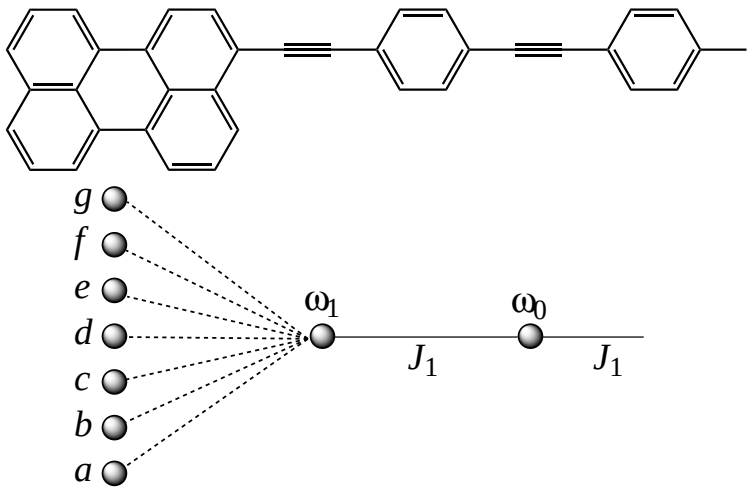

Figure 5.17: Perylene terminated linear phenylacetylene molecules and the relevant lattice model.

From the quantum-chemical (CEO) results of a set of linear PA molecules with one end substituted by perylene, we observed three bound exciton states localized in the vicinity of the perylene: one state below the exciton band whereas the other two above the band. The exciton wave function extracted from the transition density matrix can be described as an exponential decay with complex wave numbers. Therefore the wave number could be found from the exponential fit of the wave function.

We also observed four additional resonant states inside the exciton band which correspond to the kink features of the reflection phase shown in Fig.5.18. The reflection phase is calculated using Eq. (4.8). Since the resonant state can be interpreted as the superposition of an excitation localized at perylene and the standing wave with reduced amplitudes in the chain, the excited states of single perylene molecule have been computed to compare with the later tight-binding model.

The complexity of the reflection phase of perylene makes it difficult to determine the lattice structure from the profile of the phase because several bound states and resonance states have been introduced simultaneously. However, once the phase is obtained as a function of exciton momentum k, analytic continuation can be technologically done to provide

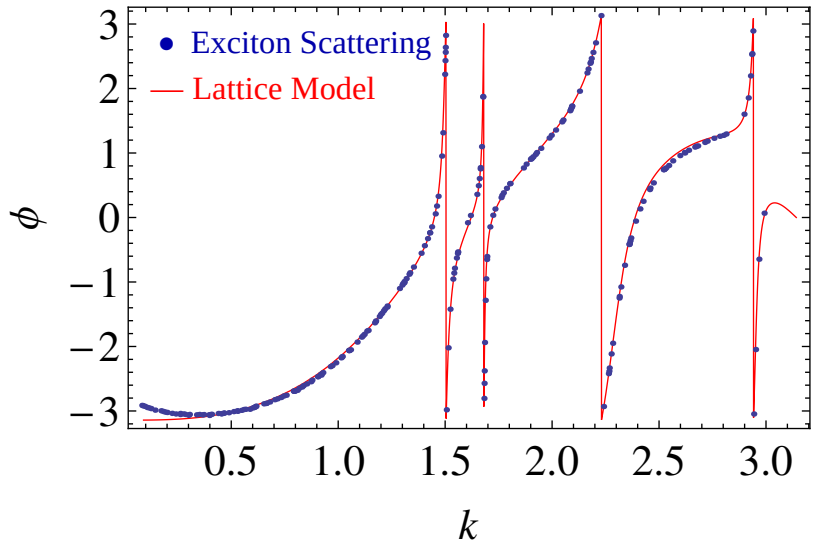

Figure 5.18: The reflection phase of the perylene substituted terminus in phenylacetylene molecules.

information about the bound states. Combined with the topological charge Q directly from the $\phi(k)$, the structure of the tight-binding model could be determined in principle. A quick way to build the lattice structure for a molecular vertex is from the corresponding quantum-chemical result. In our case, excitations of one linear molecule that covered the whole exciton band should be calculated. Comparing the molecular length L to the number of the states N with respect to the specific exciton type (including bound states and resonant states), the number of lattice sites is known as $N - L$. The method will not increase the computational cost since the ES approach needs the same quantum-chemical computation. In the lattice models for perylene terminated molecules, seven lattice sites are used to represent the perylene terminus as shown in Fig. 5.17. One varied on-site energy is used to characterize the nearby terminal effect.

Using the lattice model the four features of resonance in the reflection phase have been reproduced precisely, the three bound states have been predicted with respect to the exciton band since the lattice model does not approximate the dispersion very well near the band edges. The relative positions of the bound states are compared to the quantum-chemical

	bound state 1	bound state 2	bound state 3
QC method (CEO)	-0.263 eV	0.035 eV	0.175 eV
tight-binding model	-0.309 eV	0.025 eV	0.137 eV

Table 5.1: The bound states in perylene terminated molecules predicted by the tight-binding models and the quantum-chemical method. The energy distance to the nearest band edge is listed. Negative value corresponds to a bound state below the exciton band.

results in Table 5.1.

So far tight-binding model representation has been applied to all studied phenylacetylene based molecular vertices. For any molecule consists of these vertices, the corresponding lattice model can be constructed. The exciton Hamiltonian matrix can be parameterized by the relevant lattice constants. All excitation energies can be found as the eigenvalues of the Hamiltonian. Although the states near the band edges can not be predicted accurately because of the inaccurate dispersion, the states in the middle part of the band are well calculated by the tight-binding model (see the example in Fig. 5.19).

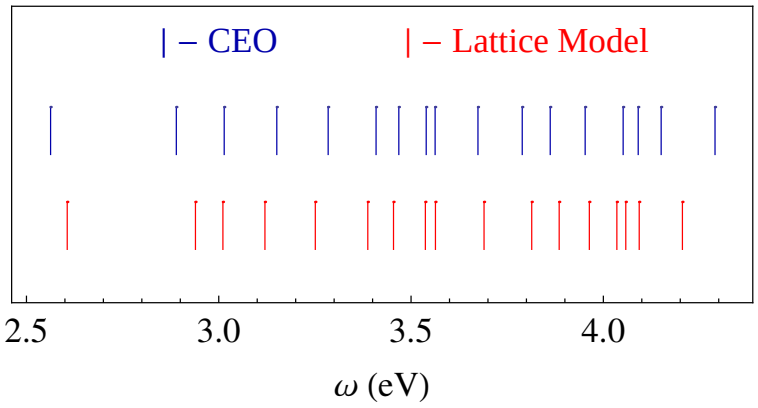

Figure 5.19: The excitation energies of the linear molecule with 10 repeat units and one end terminated by perylene.

Since now the electronic excitations in PA-based molecules have been characterized by only a small number of geometry-dependent constants, the tight-binding models can be used to parameterize the effect of geometric distortions on the excitations, which control the energy transfer timescales. The efficient tight-binding description of the exciton-phonon

interactions makes it possible to treat the photoinduced dynamics.

Chapter 6

Conclusions

Electronic excitations in branched conjugated molecules have been investigated from a quasiparticle view and using effective tight-binding models. The spectroscopic computation within the exciton scattering (ES) methodology can be performed in real-time with minimum numerical cost. The tight-binding representation explicitly characterizes the electronic excitations, and provides an applicable treatment of photoinduced dynamics following the incorporation of exciton-phonon interactions.

The formalism of the (ES) approach [36, 39, 42–44] for electronic excitations in branched conjugated molecules has been generalized and extended to calculation of oscillator strengths. Together with the original ES approach, this extension allows one to calculate efficiently optical spectra in large conjugated molecules using previously tabulated ES parameters obtained from quantum-chemical calculations of basic molecular building blocks. The ES approach can be applied to conjugated molecules where electronic excitations are tightly bound spatially localized excitons. In the ES model, they are viewed as quasiparticles on the graph that represents the molecule (the molecular vertices and linear segments are represented by the vertices and edges of the graph). Within the ES approach we assume that the properties of the molecular building blocks (repeat units and molecular vertices) depend only on the energy. The excited state energies and distributions of the excitation amplitude are found within the ES approach by solving a generalized "particle in a box" problem on the graph with the given exciton dispersion relation and scattering matrices. In addition, we intro-

duce the transition charge and dipole parameters of the ES approach that characterize how contributions of building blocks to the total transition dipole depend on the local excitation amplitudes. The ES parameters of the building blocks can be extracted from the results of quantum-chemical computations in relatively small molecular fragments.

The effects of chemical substitutions with donor and acceptor moieties can be naturally incorporated into the ES framework. Within the ES approach, these chemical modifications change the energy-dependent ES parameters of the substituents. The parameters, included in the ES library, enable efficient computation of electronic spectra in a wide variety of phenylacetylene-based molecules. In addition to accurate and less expensive numerical predictions, the ES model is useful for qualitative understanding of the excited-state electronic structure.

The exciton scattering properties of the symmetric double, triple and quadruple joints, referred to as V-, Y- and X-joints, respectively, have been characterized with the scatting matrices according to their symmetries. The relevant phases parameterizing the matrices have been retrieved from quantum chemistry calculations. The relations between the number of the in-band excitations, the molecular length, and characteristic features of the scattering phases, have been formulated as functions of the quasi-momentum. This knowledge guaranteed the adequate representation of molecular vertices within tight-binding models.

The effective tight-binding (lattice) models have been developed to simplify the description of the excitonic states in conjugated molecules. It allows one to do analytic continuations of scattering matrices and predict the out-band bound exciton states. The lattice parameters are retrieved from exciton scattering analysis and are only geometry-dependent. The effect of geometric distortion can be treated by such lattice models. With the derived exciton-phonon Hamiltonian the photoinduced dynamics in realistic structures can be studied.

BIBLIOGRAPHY

[1] C. Wu. *Excited states of branched conjugated molecules using the exciton scattering approach.* PhD thesis, Wayne State University, 2009.

[2] F. Diederich. Carbon scaffolding: building acetylenic all-carbon and carbon-rich compounds. *Nature*, 369:199–207, 1994.

[3] R. H. Baughman, H. Eckhardt, and M. Kertesz. Structure-property predictions for new planar forms of carbon: Layered phases containing sp^2 and sp atoms. *Journal of Chemical Physics*, 87(11):6687–6699, 1987.

[4] U. H. F. Bunz. Synthesis and structure of paes. *Advances in Polymer Science*, 177:1–52, 2005.

[5] W. Zhang and J. S. Moore. Shape-persistent macrocycles: Structures and synthetic approaches from arylene and ethynylene building blocks. *Angewandte Chemie International Edition*, 45(27):4416–4439, 2006.

[6] E. L. Spitler, C. A. Johnson II, and M. M. Haley. Renaissance of annulene chemistry. *Chemical Reviews*, 106(12):5344–5386, 2006.

[7] Z. H. Peng, J. S. Melinger, and V. Kleiman. Light harvesting unsymmetrical conjugated dendrimders as photosynthetic mimics. *Photosynthesis Research*, 87(1):115–131, 2006.

[8] R. Kopelman, M. Shortreed, Z. Y. Shi, W. H. Tan, Z. F. Xu, J. S. Moore, A. BarHaim, and J. Klafter. Spectroscopic evidence for excitonic localization in fractal antenna supermolecules. *Physical Review Letters*, 78(7):1239–1242, 1997.

[9] C. Devadoss, P. Bharathi, and J. S. Moore. Energy transfer in dendritic macromolecules: molecular size effects and the role of an energy gradient. *Journal of the Americal*

Chemical Society, 118:9635–9644, 1996.

[10] T. G. Goodson. Optical excitations in organic dendrimers investigated by time-resolved and nonlinear optical spectroscopy. *Accounts of Chemical Research*, 38(2):99–107, 2005.

[11] A. Bhaskar, R. Guda, M. M. Haley, and T. G. Goodson. Building symmetric two-dimensional two-photon materials. *Journal of the American Chemical Society*, 128(43):13972–13973, 2006.

[12] P. F. Barbara, A. J. Gesquiere, S. J. Park, and Y. J. Lee. Single-molecule spectroscopy of conjugated polymers. *Accounts of Chemical Research*, 38(7):602–610, 2005.

[13] A. J. Heeger. Nobel lecture: Semiconducting and metallic polymers: The fourth generation of polymeric materials. *Reviews of Modern Physics*, 73:681–700, 2001.

[14] A. J. Heeger, S. Kivelson, J. R. Schrieffer, and W. P. Su. Solitons in conducting polymers. *Reviews of Modern Physics*, 60(3):781–850, 1988.

[15] K. I. Igumenshchev, S. Tretiak, and V. Y. Chernyak. Excitonic effects in a time-dependent density functional theory. *Journal of Chemical Physics*, 127(11), 2007.

[16] R. H. Friend, R. W. Gymer, A. B. Holmes, J. H. Burroughes, R. N. Marks, C. Taliani, D. D. C. Bradley, D. A. Dos Santos, J. L. Bredas, M. Logdlund, and W. R. Salaneck. Electroluminescence in conjugated polymers. *Nature*, 397:121–128, 1999.

[17] F. Schindler, J. M. Lupton, J. Muller, and U. Feldmann, J.and Scherf. How single conjugated polymer molecules respond to electric fields. *Nature Materials*, 5:141–146, 2006.

[18] S. Gunes, H. Neugebauer, and N. S. Sariciftci. Conjugated polymer-based organic solar cells. *Chemical Reviews*, 107(4):1324–1338, 2007.

[19] Y. Yang and A. J. Heeger. A new architecture for polymer transistors. *Nature*, 372:344–346, 1994.

[20] A. R. Murphy and J. M. J. Frechet. Organic semiconducting oligomers for use in thin film transistors. *Chemical Reviews*, 107:1066–1096, 2007.

[21] H. Sirringhaus, T. Kawase, R. H. Friend, T. Shimoda, M. Inbasekaran, W. Wu, and

E. P. Woo. High-resolution inkjet printing of all-polymer transistor circuits. *Science*, 290:2123–2126, 2000.

[22] A. J. Heeger, D. J. Heeger, J. Langan, and Y. Yang. Image enhancement with polymer grid triode arrays. *Science*, 270:1642–1644, 1995.

[23] E. Menard, M. A. Meitl, Y. Sun, J.-U. Park, D. J.-L. Shir, Y.-S. Nam, S. Jeon, and J. A. Rogers. Micro- and nanopatterning techniques for organic electronic and optoelectronic systems. *Chemical Reviews*, 107:1117–1160, 2007.

[24] T. M. Figueira-Duarte, A. Gegout, and J. F. Nierengarten. Molecular and supramolecular C-60-oligophenylenevinylene conjugates. *Chemical Communications*, (2):109–119, 2007.

[25] N. Kopidakis, W. J. Mitchell, J. van de Lagemaat, D. S. Ginley, G. Rumbles, S. E. Shaheen, and W. L. Rance. Bulk heterojunction organic photovoltaic devices based on phenyl-cored thiophene dendrimers. *Applied Physics Letters*, 89(10), 2006.

[26] A. J. Berresheim, M. Muller, and K. Mullen. Polyphenylene nanostructures. *Chemical Reviews*, 99(7):1747–1786, 1999.

[27] J. Locklin, D. Patton, S. Deng, A. Baba, M. Millan, and R. C. Advincula. Conjugated oligothiophene-dendron-capped CdSe nanoparticles: Synthesis and energy transfer. *Chemistry of Materials*, 16(24):5187–5193, 2004.

[28] V. Percec, M. Glodde, T. K. Bera, Y. Miura, I. Shiyanovskaya, K. D. Singer, V. S. K. Balagurusamy, P. A. Heiney, I. Schnell, A. Rapp, H. W. Spiess, S. D. Hudson, and H. Duan. Self-organization of supramolecular helical dendrimers into complex electronic materials. *Nature*, 417(6905):384–387, 2002.

[29] Z. H. Peng, Y. C. Pan, B. B. Xu, and J. H. Zhang. Synthesis and optical properties of novel unsymmetrical conjugated dendrimers. *Journal of the American Chemical Society*, 122(28):6619–6623, 2000.

[30] D. A. Tomalia, A. M. Naylor, and W. A. Goddard. Starburst dendrimers - molecular-level control of size, shape, surface-chemistry, topology, and flexibility from atoms to

macroscopic matter. *Angewandte Chemie-International Edition in English*, 29(2):138–175, 1990.

[31] D. Gust, T. A. Moore, and A. L. Moore. Mimicking photosynthetic solar energy transduction. *Accounts of Chemical Research*, 34(1):40–48, 2001.

[32] T. S. Ahn, A. L. Thompson, P. Bharathi, A. Muller, and C. J. Bardeen. Light-harvesting in carbonyl-terminated phenylacetylene dendrimers: The role of delocalized excited states and the scaling of light-harvesting efficiency with dendrimer size. *Journal of Physical Chemistry B*, 110(40):19810–19819, 2006.

[33] J. Y. Kim, K. Lee, N. E. Coates, D. Moses, T. Q. Nguyen, M. Dante, and A. J. Heeger. Efficient tandem polymer solar cells fabricated by all-solution processing. *Science*, 317(5835):222–225, 2007.

[34] B. C. Thompson and J. M. J. Frechet. Organic photovoltaics - polymer-fullerene composite solar cells. *Angewandte Chemie-International Edition*, 47(1):58–77, 2008.

[35] A. Adronov and J. M. J. Frechet. Light-harvesting dendrimers. *Chemical Communications*, (18):1701–1710, 2000.

[36] C. Wu, S. V. Malinin, S. Tretiak, and V. Y. Chernyak. Exciton scattering and localization in branched dendrimeric structures. *Nature Physics*, 2(9):631–635, 2006.

[37] J. Yu, D. H. Hu, and P. F. Barbara. Unmasking electronic energy transfer of conjugated polymers by suppression of O_2 quenching. *Science*, 289(5483):1327–1330, 2000.

[38] C. J. Cramer. *Computational Chemistry*. John Wiley & Sons, Chichester, 2004.

[39] C. Wu, S. V. Malinin, S. Tretiak, and V. Y. Chernyak. Multiscale modeling of electronic excitations in branched conjugated molecules using an exciton scattering approach. *Physical Review Letters*, 100(5):057405, 2008.

[40] V. Chernyak, S. N. Volkov, and S. Mukamel. Exciton coherence and electron energy loss spectroscopy of conjugated molecules. *Physical Review Letters*, 86(6):995–998, 2001.

[41] V. Chernyak, S. N. Volkov, and S. Mukamel. Electronic structure-factor, density matrices, and electron energy loss spectroscopy of conjugated oligomers. *Journal of Physical*

Chemistry A, 105(10):1988–2004, 2001.

[42] C. Wu, S. V. Malinin, S. Tretiak, and V. Y. Chernyak. Exciton scattering approach for branched conjugated molecules and complexes. I. Formalism. *Journal of Chemical Physics*, 129:174111, 2008.

[43] C. Wu, S. V. Malinin, S. Tretiak, and V. Y. Chernyak. Exciton scattering approach for branched conjugated molecules and complexes. II. Extraction of the exciton scattering parameters from quantum-chemical calculations. *Journal of Chemical Physics*, 129:174112, 2008.

[44] C. Wu, S. V. Malinin, S. Tretiak, and V. Y. Chernyak. Exciton scattering approach for branched conjugated molecules and complexes. III. Applications. *Journal of Chemical Physics*, 129:174113, 2008.

[45] S. Mukamel. *Principles of Nonlinear Optical Spectroscopy*. Oxford University Press, New York, 1995.

[46] S. Tretiak and S. Mukamel. Density matrix analysis and simulation of electronic excitations in conjugated and aggregated molecules. *Chemical Reviews*, 102(9):3171–3212, 2002.

[47] S. Tretiak, A. Saxena, R. L. Martin, and A. R. Bishop. Conformational dynamics of photoexcited conjugated molecules. *Physical Review Letters*, 89(9):097402, 2002.

[48] A. Bar-Haim, J. Klafter, and R. Kopelman. Dendrimers as controlled artificial energy antennae. *Journal of the American Chemical Society*, 119(26):6197–6198, 1997.

[49] W. Ortiz, B. P. Krueger, V. D. Kleiman, J. L. Krause, and A. E. Roitberg. Energy transfer in the nanostar: The role of coulombic coupling and dynamics. *Journal of Physical Chemistry B*, 109(23):11512–11519, 2005.

[50] D. G. Kuroda, C. P. Singh, Z. Peng, and V. D. Kleiman. Mapping excited-state dynamics by coherent control of a dendrimers photoemission efficiency. *Science*, 326(5950):263–267, 2009.

[51] E. R. Davidson. *Reduced Density Matrices in Quantum Chemistry*. Academic Press,

New York, 1976.

[52] M. E. Casida. *Recent Advances in Density Functional Methods Part I.* World Scientific Press, Singapore, 1995.

[53] E. Runge and E. K. U. Gross. Density-functional theory for time-dependent systems. *Physical Review Letters*, 52(12):997–1000, 1984.

[54] D. Pines and D. Bohm. A collective description of electron interactions: Ii. collective vs individual particle aspects of the interactions. *Physical Review*, 85(2):338–353, 1952.

[55] D. J. Thouless. Vibrational states of nuclei in the random phase approximation. *Nuclear Physics*, 22(1):78–95, 1961.

[56] A. Szabo and N. S. Ostlund. *Modern Quantum Chemistry: Introduction to Advanced Electronic Structure Theory.* McGraw-Hill, New York, 1989.

[57] E. K. U. Gross, J. F. Dobson, and M. Petersilka. *Density Functional Theory II*, volume 181 of *Topics in Current Chemistry.* Springer, Berlin, 1996.

[58] W. Koch and M. C. Holthausen. *A Chemists Guide to Density Functional Theory.* Wiley-VCH, Weinheim, 2000.

[59] A. Dreuw and M. Head-Gordon. Single-reference ab initio methods for the calculation of excited states of large molecules. *Chemical Review*, 105(11):4009–4037, 2005.

[60] D. B. Cook. *Handbook of Computational Quantum Chemistry.* Oxford University Press, New York, 1998.

[61] M. J. S. Dewar, E. G. Zoebisch, E. F. Healy, and J. J. P. Stewart. AM1: a new general purpose quantum mechanical molecular model. *Journal of The American Chemical Society*, 107(13):3902–3909, 2002.

[62] M. J. Frisch, G. W. Trucks, H. B. Schlegel, G. E. Scuseria, M. A. Robb, J. R. Cheeseman, J. A. Montgomery, T. Jr., Vreven, K. N. Kudin, J. C. Burant, J. M. Millam, S. S. Iyengar, J. Tomasi, V. Barone, B. Mennucci, M. Cossi, G. Scalmani, N. Rega, G. A. Petersson, H. Nakatsuji, M. Hada, M. Ehara, K. Toyota, R. Fukuda, J. Hasegawa, M. Ishida, T. Nakajima, Y. Honda, O. Kitao, H. Nakai, M. Klene, X. Li, J. E. Knox,

H. P. Hratchian, J. B. Cross, V. Bakken, C. Adamo, J. Jaramillo, R. Gomperts, R. E. Stratmann, O. Yazyev, A. J. Austin, R. Cammi, C. Pomelli, J. W. Ochterski, P. Y. Ayala, K. Morokuma, G. A. Voth, P. Salvador, J. J. Dannenberg, V. G. Zakrzewski, S. Dapprich, A. D. Daniels, M. C. Strain, O. Farkas, D. K. Malick, A. D. Rabuck, K. Raghavachari, J. B. Foresman, J. V. Ortiz, Q. Cui, A. G. Baboul, S. Clifford, J. Cioslowski, B. B. Stefanov, G. Liu, A. Liashenko, P. Piskorz, I. Komaromi, R. L. Martin, D. J. Fox, T. Keith, M. A. Al-Laham, C. Y. Peng, A. Nanayakkara, M. Challacombe, P. M. W. Gill, B. Johnson, W. Chen, M. W. Wong, C. Gonzalez, and J. A. Pople. *GAUSSIAN 03 (Revision C.02)*. Gaussian, Inc., Wallingford, CT, 2004.

[63] S. Mukamel, S. Tretiak, T. Wagersreiter, and V. Chernyak. Electronic coherence and collective optical excitations of conjugated molecules. *Science*, 277(5327):781–787, 1997.

[64] S Tretiak, V Chernyak, and S Mukamel. Localized electronic excitations in phenylacetylene dendrimers. *Journal of Physical Chemistry B*, 102(18):3310–3315, 1998.

[65] H. Li, S. V. Malinin, S. Tretiak, and V. Y. Chernyak. Exciton scattering approach for branched conjugated molecules and complexes. IV. Transition dipoles and optical spectra. *Journal of Chemical Physics*, 132:124103, 2010.

[66] D. R. Larson, W. R. Zipfel, R. M. Williams, S. W. Clark, M. P. Bruchez, F. W. Wise, and W. W. Webb. Water-soluble quantum dots for multiphoton fluorescence imaging in vivo. *Science*, 300(5624):1434–1436, 2003.

[67] S. Kawata, H.-B. Sun, T. Tanaka, and Takada K. Finer features for functional microdevices. *Nature*, 412:697–698, 2001.

[68] D. A. Parthenopoulos and P. M. Rentzepis. Three-dimensional optical storage memory. *Science*, 245:843–845, 1989.

[69] W. Zhou, S. M. Kuebler, K. L. Braun, T. Yu, J. K. Cammack, C. K. Ober, J. W. Perry, and S. R. Marder. An efficient two-photon-generated photoacid applied to positive-tone 3d microfabrication. *Science*, 296(5570):1106–1109, 2002.

[70] B. H. Cumpston, S. P. Ananthavel, S. Barlow, D. L. Dyer, J. E. Ehrlich, L. L. Ersk-

ine, A. A. Heikal, S. M. Kuebler, I.-Y. S. Lee, D. McCord-Maughon, J. Qin, H. Rckel, M. Rumi, X.-L. Wu, S. R. Marder, and J. W. Perry. Two-photon polymerization initiators for three-dimensional optical data storage and microfabrication. *Nature*, 398:51–54, 1999.

[71] C Wu, S. Tretiak, and V Chernyak. Excited states and optical response of a donor-acceptor substituted polyene: a TDDFT study. *Chemical Physics Letters*, 433:305–311, 2007.

[72] O. Mongin, L. Porrs, M. Charlot, C. Katan, and M. Blanchard-Desce. Synthesis, fluorescence, and two-photon absorption of a series of elongated rodlike and banana-shaped quadrupolar fluorophores: A comprehensive study of structureproperty relationships. *Chemistry - A European Journal*, 13(5):1481–1498, 2007.

[73] H. Meier. Conjugated oligomers with terminal donor-acceptor substitution. *Angewandte Chemie International Edition*, 44:2482–2506, 2005.

[74] P. N. Prasad. *Introduction to Biophotonics*. Wiley Interscience, New York, 2003.

[75] P. N. Prasad. *Nanophotonics*. Wiley Interscience, New York, 2004.

[76] S Tretiak, V Chernyak, and S Mukamel. Two-dimensional real-space analysis of optical excitations in acceptor-substituted carotenoids. *Journal of the American Chemical Society*, 119(47):11408–11419, 1997.

[77] A. M. Moran, A. M. Kelly, and S Tretiak. Excited state molecular dynamics simulations of nonlinear push-pull chromophores. *Chemical Physics Letters*, 367:293–307, 2003.

[78] W. H. Thompson, M. Blanchard-Desce, and J. T. Hynes. Two valence bond state model for molecular nonlinear optical properties. nonequilibrium solvation formulation. *Journal of Physical Chemistry A*, 102:7712–7722, 1998.

[79] G. Malliaras and R. Friend. An organic electronics primer. *Physics Today*, May 2005:53–58, 2005.

[80] H. Li, C. Wu, S. V. Malinin, S. Tretiak, and V. Y. Chernyak. Excited states of donor and acceptor substituted conjugated oligomers: A perspective from the exciton scattering

approach. *Journal of Physical Chemistry Letters*, 1:3396–3400, 2010.

[81] L. D. Landau and E. M. Lisfshitz. *Quantum Mechanics (Non-Relativistic Theory), Volume 3*. Pergamon Press, 1991.

[82] M. C. Zerner. Zindo: A semi-empirical quantum chemistry program. In *Quantum Theory Project*. University of Florida, Gainesville, FL, 1991.

[83] S. Tretiak, K. Igumenshchev, and V. Chernyak. Exciton sizes of conducting polymers predicted by time-dependent density functional theory. *Physical Review B*, 71(3):033201, 2005.

[84] R. J. Magyar, S. Tretiak, Y. Gao, H. L. Wang, and A. P. Shreve. A joint theoretical and experimental study of phenylene-acetylene molecular wires. *Chemical Physics Letters*, 401(1-3):149–156, 2005.

[85] E. Moore, B. Gherman, and D. Yaron. Coulomb screening and exciton binding energies in conjugated polymers. *Journal of Chemical Physics*, 106:4216–4227, 1997.

[86] M. W. Hirsch. *Differential Topology*. Springer, 1997.

[87] T Minami, S Tretiak, V Chernyak, and S Mukamel. Frenkel-exciton Hamiltonian for dendrimeric nanostar. *Journal of Luminescence*, 87-9:115–118, 2000.

[88] H. Fidder, J. Knoester, and D. A. Wiersma. Optical properties of disordered molecular aggregates: A numerical study. *Journal of Chemical Physics*, 95(11):7880–7890, 1991.

[89] H. Li, C. Wu, S. V. Malinin, S. Tretiak, and V. Y. Chernyak. Exciton scattering on symmetric branching centers in conjugated molecules. *(in press) Journal of Physical Chemistry B*, 2011.

[90] M. R. Shortreed, S. F. Swallen, Z-. Y. Shi, W. Tan, Z. Xu, C. Devadoss, J. S. Moore, and R. Kopelman. Directed energy transfer funnels in dendrimeric antenna supermolecules. *Journal of Physical Chemistry B*, 101:6318–6322, 1997.

ABSTRACT

ELECTRONIC EXCITATIONS IN BRANCHED CONJUGATED OLIGOMERS: A QUASIPARTICLE VIEW AND TIGHT-BINDING MODELS

by

HAO LI

August 2011

Advisor: Vladimir Y. Chernyak

Major: Chemistry (Physical)

Degree: Doctor of Philosophy

This dissertation focuses on the theoretical understanding and simulation of the excited state electronic structures of organic conjugated molecules. The exciton scattering (ES) approach has been extended for efficient calculation of optical spectra of large branched conjugated oligomers. The methodology of tight-binding (lattice) model, originally developed in condensed matter theory, has been extended to the building block structure of conjugated molecules for explicit description of the electronic excitations.

Within the ES approach, the electronic excitations in quasi-1D molecular structures are attributed to standing waves that represent quantum quasiparticles (excitons) scattered at the molecular vertices. Excitation energies can be found by solving a generalized "particle in the box" problem on the graph that represents the molecule. The transition dipoles can be calculated by counting dipole contribution of each molecular building block, which is proportional to the amplitude of the excitation. The ES methodology is also extended to analyze the electronic excitations in oligomers with electron donor and acceptor substituents, which are known to modify the electronic and optical properties. The energy-dependent ES parameters that characterize the exciton properties on building blocks can be extracted from quantum chemical computations in simple molecular segments and tabulated for further applications. This methodology greatly simplifies the spectroscopic calculation for any

branched conjugated molecule that consists of characterized building blocks. The optical spectra predicted using the ES approach accurately reproduce the results of the corresponding quantum chemistry.

We introduce effective tight-binding models to describe exciton scattering in the imperfect geometries where the translational symmetry is violated by conformational distortions. The geometry-dependent parameters of lattice models including on-site energies and hopping constants are determined from the exciton scattering analysis. The tight-binding representation provides immediate analytic continuations of the scattering matrix, allows for the identification of the excitation, with complex wavenumbers, bound at the scattering center. The approach of tight-binding models, which simplify the description of the excited state electronic structure using a small number of constants, is useful to characterize the effect of geometric distortions on the excitations.

AUTOBIOGRAPHICAL STATEMENT

HAO LI

Education

05/2011 Ph.D., Chemistry (expected), Wayne State University.
07/2004 M.S., Polymer Science, University of Science and Technology of China.
07/2000 B.E., Polymer Science, University of Science and Technology of China.

Awards and Honors

2008 Departmental citation for excellence in teaching service, Wayne State University
2005 Outstanding paper prize of Journal of Chemistry Online
2003 The China Association for Instrumental Analysis Science and Technology prize
2002 Guanghua Education Scholarship

Recent Publications

1. H. Li, C. Wu, S. V. Malinin, S. Tretiak, and V. Y. Chernyak, "Exciton scattering approach for optical spectra of branched conjugated molecules", in preparation (invited), *Acc. Chem. Res.*
2. H. Li, S. V. Malinin, S. Tretiak, and V. Y. Chernyak, "Effective tight-binding models describe the exciton scattering in branched conjugated molecules", in preparation.
3. H. Li, S. V. Malinin, S. Tretiak, and V. Y. Chernyak, "Tight-binding models based on the exciton scattering approach in branched conjugated oligomers", in preparation.
4. H. Li, C. Wu, S. V. Malinin, S. Tretiak, and V. Y. Chernyak, "Exciton scattering on symmetric branching centers in conjugated molecules", accepted by *J. Phys. Chem. B*, (2010).
5. H. Li, C. Wu, S. V. Malinin, S. Tretiak, and V. Y. Chernyak, "Excited states of donor and acceptor substituted conjugated oligomers: a perspective from the Exciton Scattering Approach", *J. Phys. Chem. Lett.*, **1**, 3396-3400 (2010).
6. H. Li, S. V. Malinin, S. Tretiak, and V. Y. Chernyak, "Exciton scattering approach for branched conjugated molecules and complexes. IV. Transition dipoles and optical spectra", *J. Chem. Phys.*, **132**, 124103 (2010).

Presentations

1. *"Electronic excitations in branched conjugated molecules: a quasiparticle view and tight-binding models"*, (invited seminar), Los Alamos National Laboratory, Los Alamos, NM, February 2011.
2. *"Exciton scattering approach for optical spectra of branched conjugated molecules"*, Eleventh Annual Graduate Research Symposium, Wayne State University, Detroit, MI, October 2009.
3. *"Design of an automatic stopwatch system for Ubbelohde viscometer"*, (invited talk), The forth national symposium on polymer characterization, Hangzhou, China, November 2004.